Technical Innovation Submission – Team Peggie

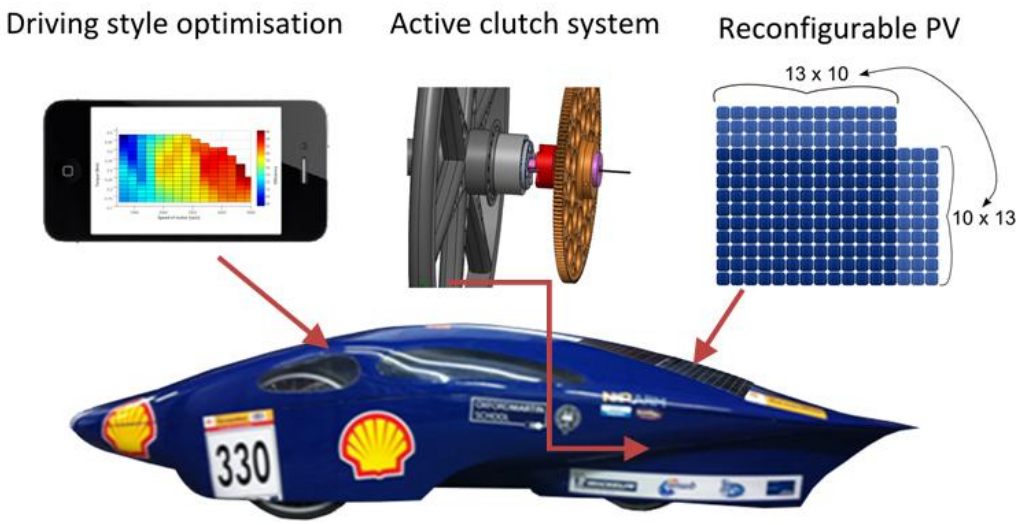

Abstract

This document presents the most innovative aspects of our team vehicle Peggie for consideration by the Shell committee. These features include:

1. A novel PV control strategy, involving a dynamically reconfigurable PV array, increases the efficiency of power conversion by 5%.
2. An innovative active clutch mechanism and control methodology, based around positional feedback of the wheel and output gear to enable phase control of the propulsion motor. This allows for engagement with minimal backlash, low actuator power requirements and reduced need for torsional compliance leading to reduced mass and losses.
3. Crucial to minimizing energy consumption is driving style. A test rig has derived a vehicle efficiency map relating to Peggie, the resulting data is processed in real-time along with track energy consumption and presented to the driver on a display integrated into the handle bars. Throttle limits on the power electronics maintains the acceleration along the most efficient trajectory.

   Track data from 2012, has been used to prime an optimisation algorithm that seeks to minimise track energy consumption subject to the constraints associated with cornering, average speed and vehicle limits. The predictions from the algorithm evolve as vehicle data, such as real time energy consumption, speed, prevailing wind and driving pattern, feeds into the software which sits on an android mobile platform.

It is hoped that the combined effect of the features above will lead to a formidable entry in this year's competition.

Contents

1. Reconfigurable PV Scheme

1.1 Introduction to Reconfigurable PV Array

This section outlines the reconfigurable PV array which has been developed for the vehicle. The scheme, illustrated in Figure 1, comprises of 130 mono-crystalline cells which are partitioned by an array of MOSFET based switching elements. The panel can be reconfigured such that the cells are arranged either as a group of 10 parallel strings, each with 13 cells in series, or 13 parallel strings with 10 cells in series.

During the race, the panel can be reconfigured such that the maximum power point associated with the panel tracks the change in battery terminal voltage. By keeping the maximum power point close to the battery terminal voltage, the efficiency of the power electronics is improved and in some instances can be bypassed altogether. This leads on average to an improvement of overall efficiency in the order of 5%.

1.2 Systems Diagram

The following systems diagram shall be discussed in this section:

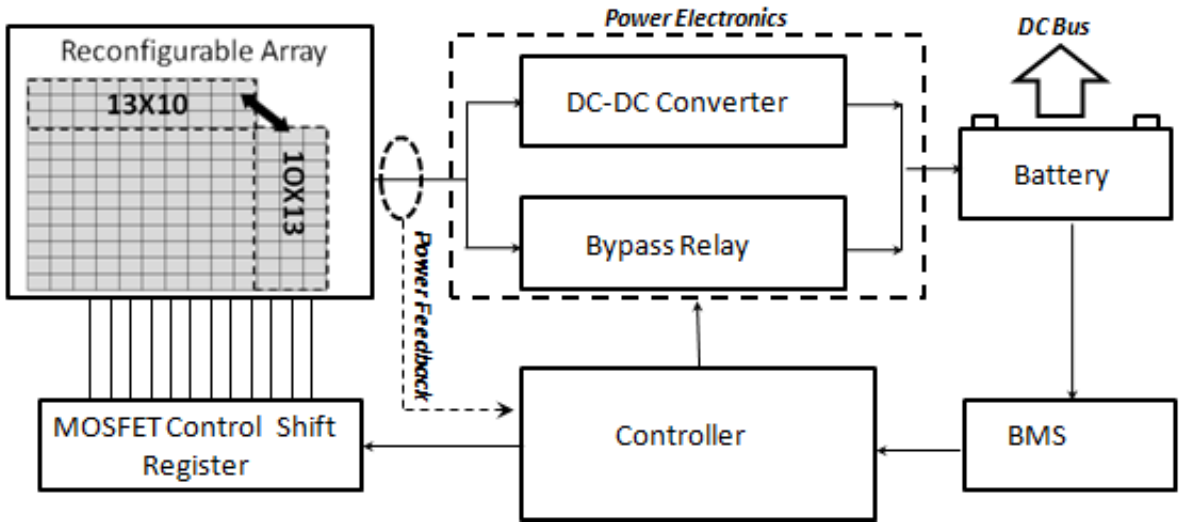

Figure 1 System Diagram Illustrating the Reconfigurable PV Array Scheme

An array of 130 photovoltaic (PV) cells are connected either in a 13X10 (series X parallel) or 10X13 configuration. The control of the configuration is implemented by an array of MOSFET based switches that are connected between the PV cells and are controlled by a shift register.

A controller decides on which configuration to implement depending on: the battery terminal voltage, feedback of power drawn from the PV array and an efficiency measurement of the DC-DC power electronics. If the BMS warns that the battery is becoming overcharged, the controller inhibits further power transfer from the power electronics.

1.3 Principle of Operation

The principle of operation is best illustrated by examination of the I-V curves associated with the photovoltaic panel against variation in battery terminal voltage. Figure 2 shows the predicted I-V and power response of the PV panel in a 13X10 configuration under a range of solar insolation values [1]:

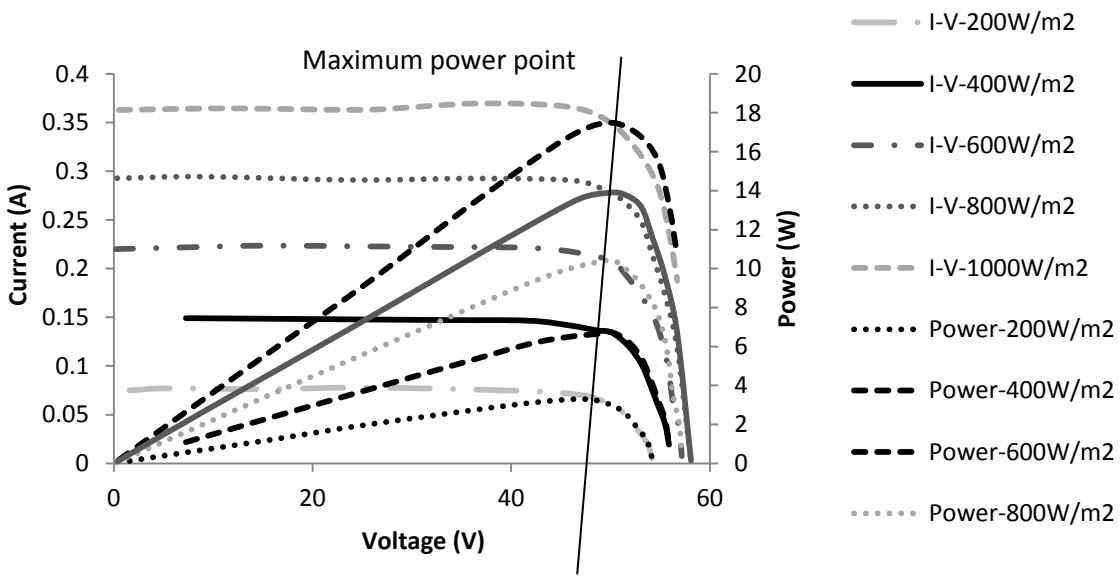

Figure 2 PV array under different levels of solar irradiation annotated to show variation in maximum power point with terminal voltage

The first observation from Figure 2 is that the maximum power point associated with the PV array varies as a function of insolation. In addition to this, the battery terminal voltage varies with state of charge. Where the battery impedance is low relative to the size of the PV array and the PV open circuit voltage is higher than the battery terminal voltage, direct connection of the PV will force the PV output to the level of the battery terminal voltage. Any disparity between the terminal voltage and PV maximum power point will lead to a loss in efficiency. To minimise this penalty, a DC-DC converter is often used so that the PV can operate continuously at the maximum power point over a wide range of battery terminal voltage and solar insolation levels. The maximum power point tracking algorithm can use one of a variety of approaches such as: perturb and observe, incremental conductance, fuzzy logic and so on, each approach has advantages and disadvantages around simplicity, accuracy, responsiveness to changes in atmospheric conditions [2] and influence of shading on the ability to track the global maximum power point [2].

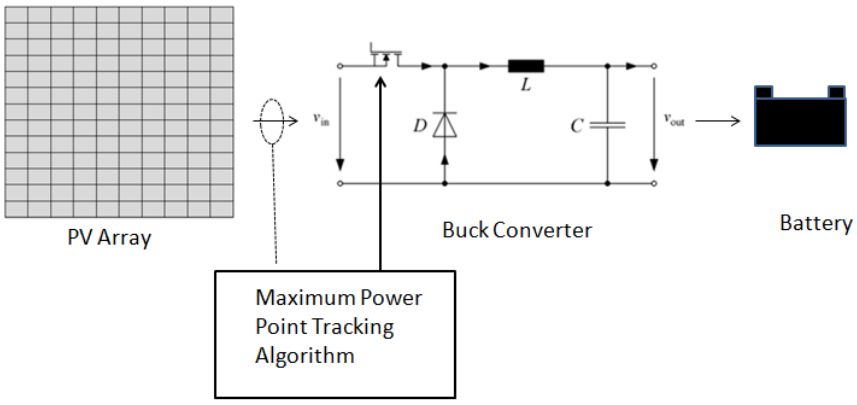

Figure 3 Typical PV power take off topology utilising DC-DC buck converter and MPPT algorithm

However, the DC-DC converter itself incurs an efficiency penalty due to the ON state resistance of the MOSFET, series resistance of the inductor and voltage drop across the diode, what's more, this penalty increases as the difference between the PV and battery terminal voltage grows [4]. This is illustrated by Figure 4 when one considers the following relationship between input voltage, V_{in}, output voltage, V_{out}, and duty cycle T for a buck converter:

$$\frac{V_{out}}{V_{in}} = D$$

Equation 1 Relationship between input voltage, output voltage and duty cycle

Where:

$$D = \frac{T_{on}}{T}$$

Equation 2 Relationship between duty cycle, on time and waveform period

For on time, T_{on} and waveform period T

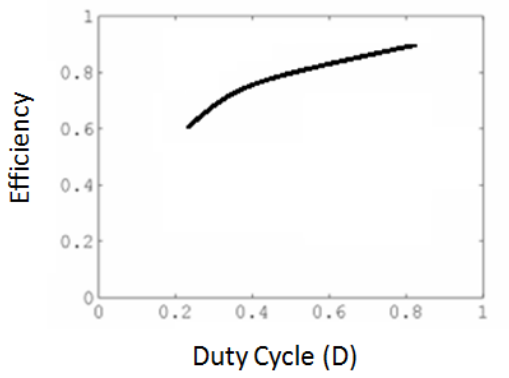

Figure 4 Typical relationship between DC-DC buck converter efficiency and duty cycle

As the ratio between output voltage and input voltage approach unity, the efficiency of the buck converter peaks. Qualitatively this can be attributed to the increasing ratio of switching time to ON time associated with the MOSFET in Figure 3 as the duty cycle drops and additional losses as current circulates through the diode during the off period. Figure 5 illustrates the losses associated with a MOSFET during switching:

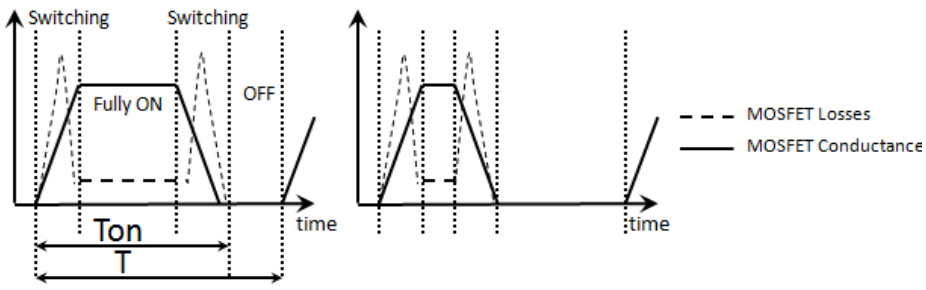

Figure 5 Illustration of influence of duty cycle on ratio of losses due to switching and useful energy transferred through a MOSFET for a give load current. Left hand waveform is associated with a high duty cycle, right hand waveform is low.

As the duty cycle decreases for a given amount of current at a given switching frequency, the proportion of time associated with switching losses, which are constant for a given current and waveform frequency, increases giving rise to reduced efficiency.

Given the relationship between input voltage, output voltage and efficiency discussed above, it is desirable to keep the voltage associated with maximum power point for the PV as close to the battery terminal voltage as possible where a DC-DC-converter is used. If the maximum power point is close enough to the terminal voltage, the DC-DC converter can be bypassed altogether. To ullustrate how this works in practice, we consider the following scenario where the battery voltage drops as the vehicle is operated:

1. **The battery is fully charged and sunlight level is 1000W/m^2**

Initially the battery is fully charged with a terminal voltage of 49V. The controller in Figure 1 configures the PV array to be in the 13 by 10 configuration to maximise the maximum power point voltage. Being so close to the battery terminal voltage, the controller computes that the efficiency penalty associated with the DC-DC converter outweighs the benefit from maximum power point tracking and so the buck converter is bypassed altogether leading to an efficiency saving in the order of 5-10%:

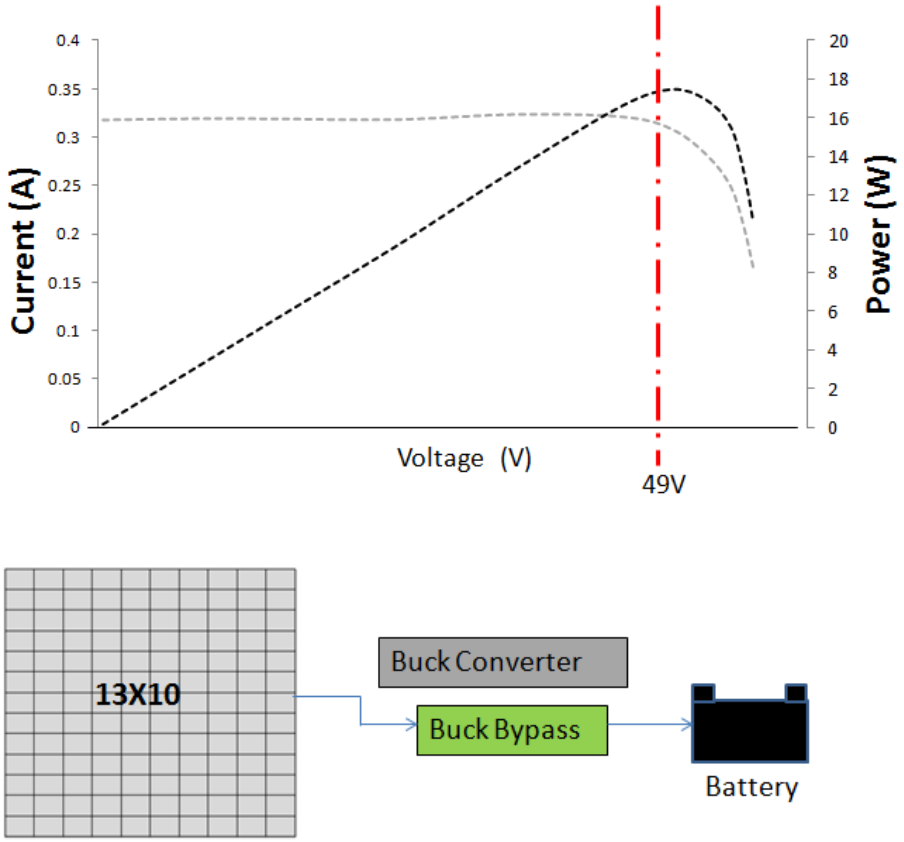

Figure 6 Configuration of PV and power electronics where battery is fully charged and irradiation = 1000W/m^2

2. Battery terminal voltage drops as the vehicle is used, sunlight level remains at 1000W/m^2

As the vehicle is used, the battery terminal drops due to the decreasing state of charge. The controller determines that the energy loss due to the difference between battery and maximum power point voltage whilst the DC-DC converter is bypassed, exceeds the loss due to the efficiency penalty associated with the power electronics, consequently the buck-converter is connected to facilitate maximum power point tracking:

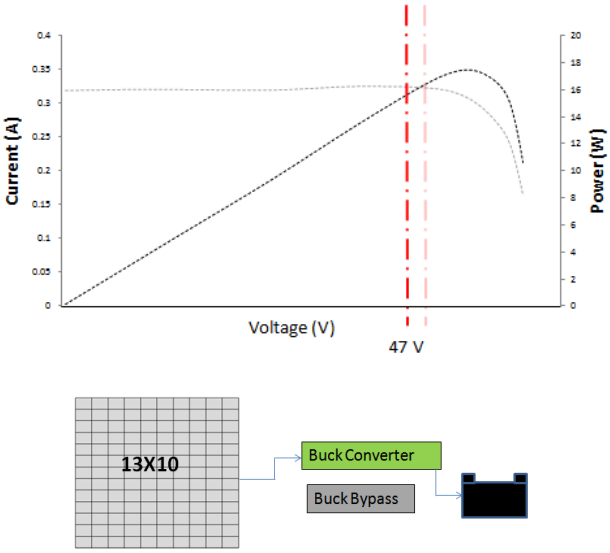

Figure 7 Configuration of PV and power electronics after first phase of battery discharge

3. Further drop in battery voltage, sunlight level – 1000W/m^2

As the battery voltage drops further, the controller deduces that reconfiguring the panel to the 10X13 configuration will manoeuvre the maximum power point so that it is closer to the battery terminal voltage. On doing this, the buck converter can be bypassed once again due to the close proximity between battery voltage and maximum power point:

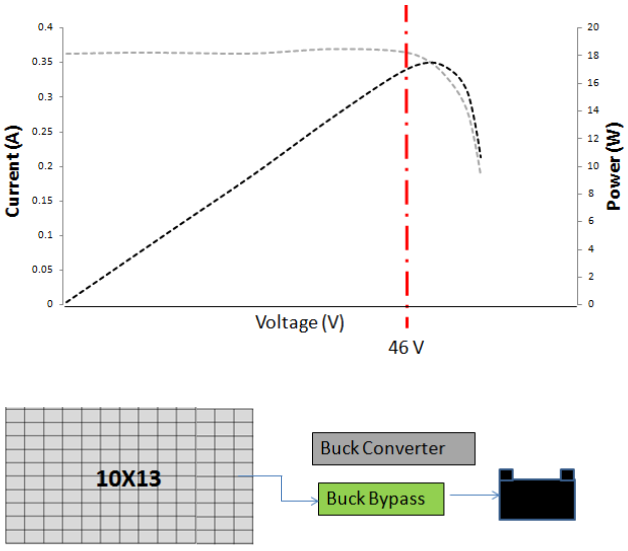

Figure 8 Change in configuration of PV due to drop in battery terminal voltage

4. **Further drop in battery voltage, sunlight level – 1000W/m^2**

As the battery voltage drops towards the minimum level, the controller reconnects the buck converter, as the PV MPPT voltage is closer to the terminal voltage than it would have been under the 13X10 configuration, the efficiency of the DC-DC converter is improved:

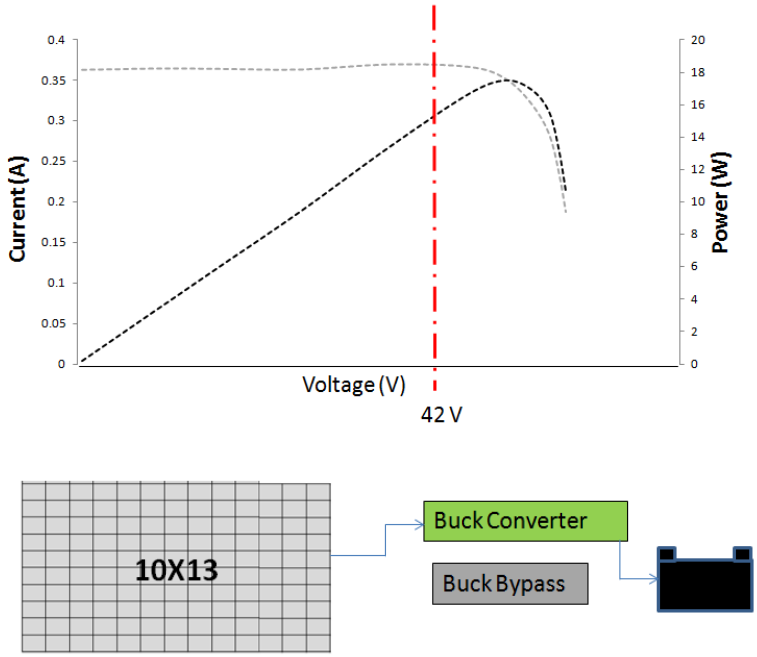

Figure 9 Configuration of panel and power electronics during final draw off from battery

1.4 Simulation of Scheme

In order to understand the likely performance advantage derived from the reconfigurable PV scheme, we consider a simulation of the circuit schematic along with operational efficiency maps.

Each of the 130 cells is simulated by the following circuit equivalent:

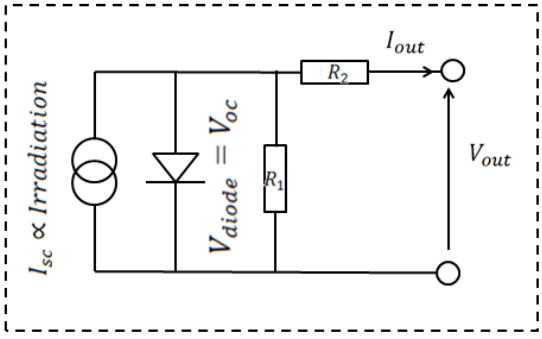

Figure 10 Circuit equivalent used for simulation of photovoltaic cells

A constant current source is set to the short circuit current, I_{sc}, associated with the level of irradiation on the PV cell. The diode forward voltage is set to the nominal open circuit voltage, V_{oc},

and resistors, R_1 and R_2 are selected so that the I-V response of the circuit matches the measured response of the PV cell. The array of 130 cells can then be simulated in one of the two following configurations:

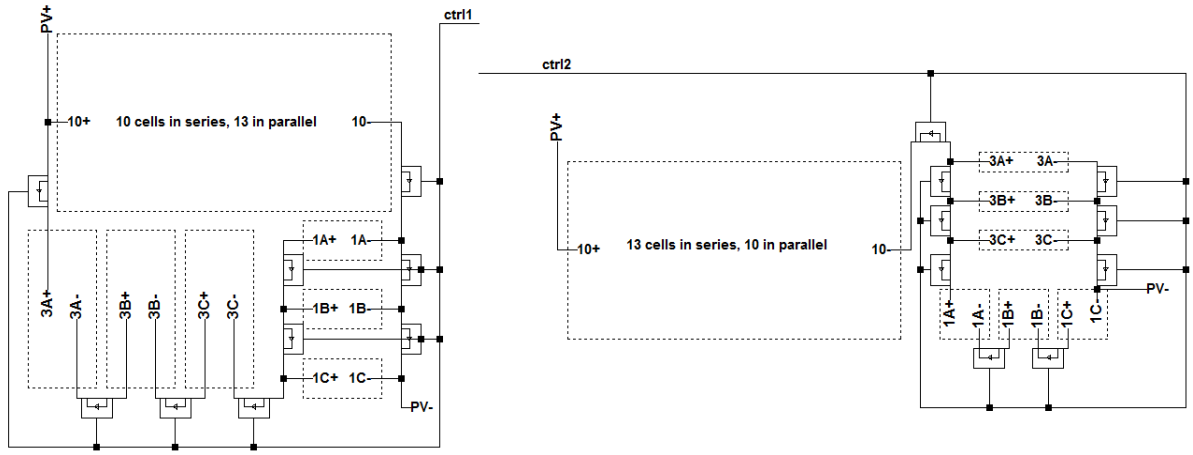

Figure 11 Reconfigurable array schematic

To select between the two configurations, switch modules detailed in the following figure are used:

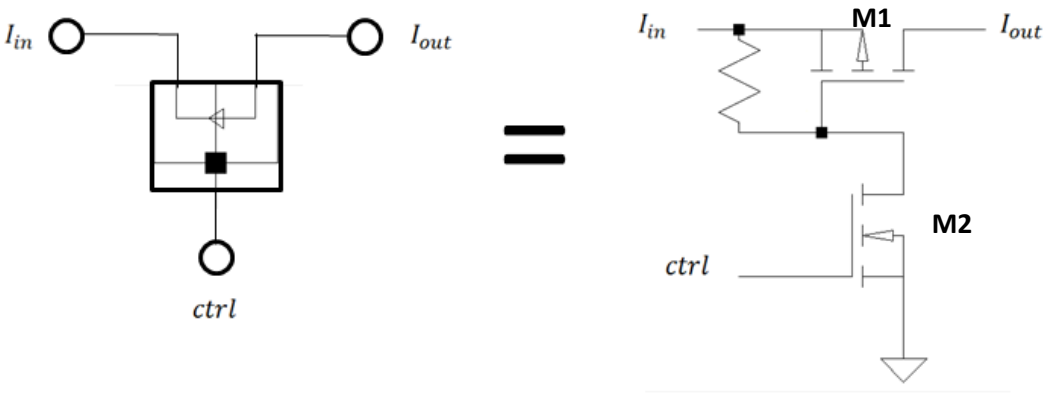

Figure 12 Switching elements within reconfigurable array

This switching arrangement ensures that MOSFET M1 is able to fully turn on or off across the full range of voltages across its respective drain and source by the pull down MOSFET, M2.

This scheme makes use of buck converter which has the following schematic:

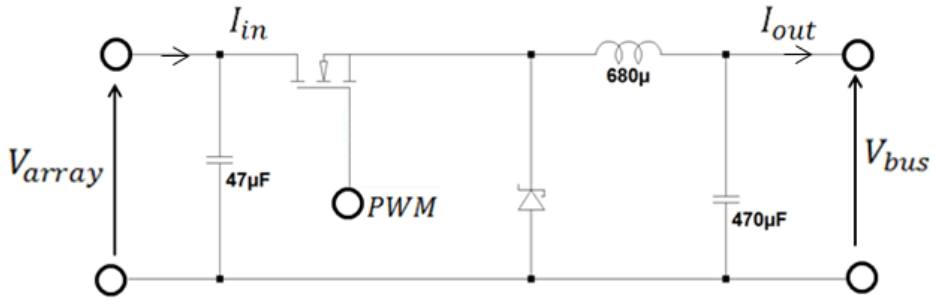

Figure 13 DC-DC converter simulated within reconfigurable PV-Scheme

The control algorithm has to decide whether or not to enable or bypass the DC-DC converter, to do this, the system model is simulated with the DC-DC converter at each operating point until the circuit has reached steady state:

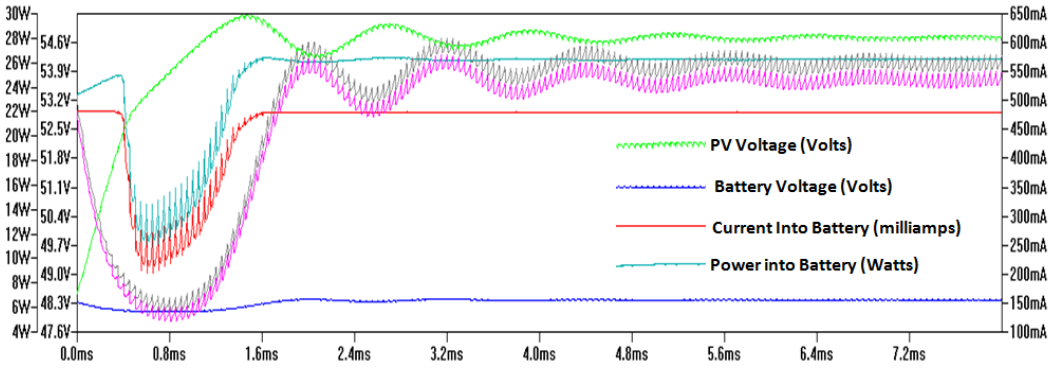

Figure 14 DC-DC converter attaining steady state during simulation of one particular operating point

Once steady state has been attained, with reference to Figure 13 and 14, the efficiency of the DC-DC converter is computed:

$$\eta_{DC-DC} = \frac{V_{array} \times I_{in}}{V_{bus} \times I_{out}} \quad (rms\ values)$$

Equation 3 Efficiency of DC-DC converter

The bypass relay is implemented by a configuration of MOSFETs as shown in Figure 12. All of the elements discussed above are simulated within the LTSPICE® environment which is particularly suited to this application [1]. A control algorithm manages the configuration of the PV array along with the PWM (Pulse Width Modulation) signal to the DC-DC converter and bypass relay control signal:

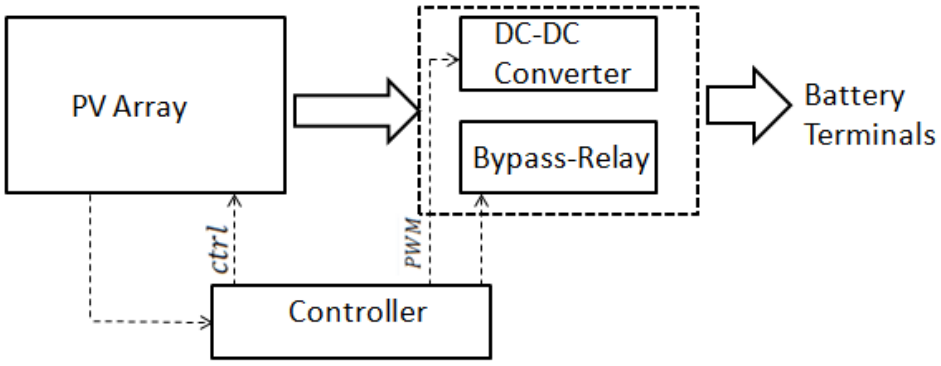

Figure 15 Simulation scheme

1.5 Simulation Results

Simulations were run over a range of battery terminal voltages and solar insolation levels to determine the overall system efficiency associated with each of the four possible system configurations:

1. 13X10 direct connection
2. 10X13 direct connection
3. 13X10 DC-DC converter
4. 10X13 DC-DC converter

The efficiency map associated with the 10X13 panel directly connected to the battery terminals is provided in Figure 16:

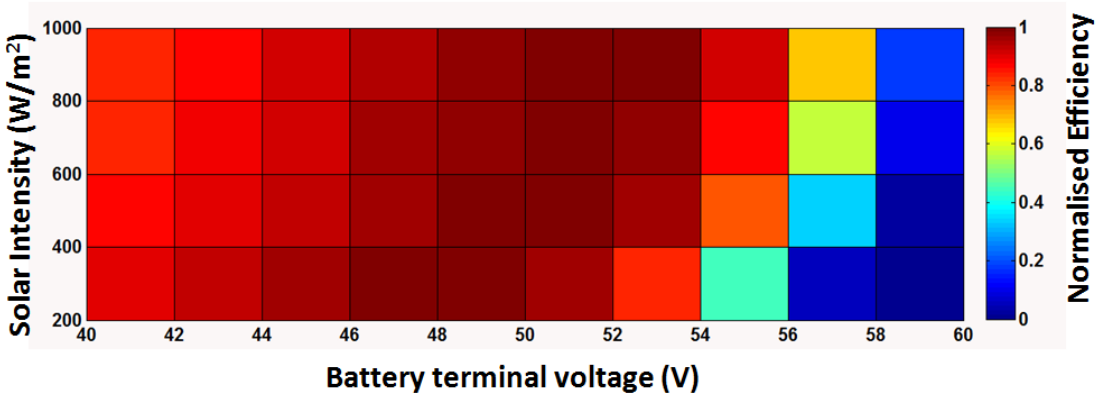

Figure 16 Efficiency map associated with direct connection of 13X10 panel configuration to battery terminals

A peak efficiency occurs around 48 to 50V where the maximum power point associated with the panel matches the terminal voltage. As the battery voltage approaches 60V, the efficiency of direct connection drops to zero due to the fact that the open circuit voltage of the panel is less than the battery terminal voltage meaning that no current can flow from the panel to the batteries. In this scenario, the panel would be reconfigured to a 13X10 arrangement which has the following efficiency map:

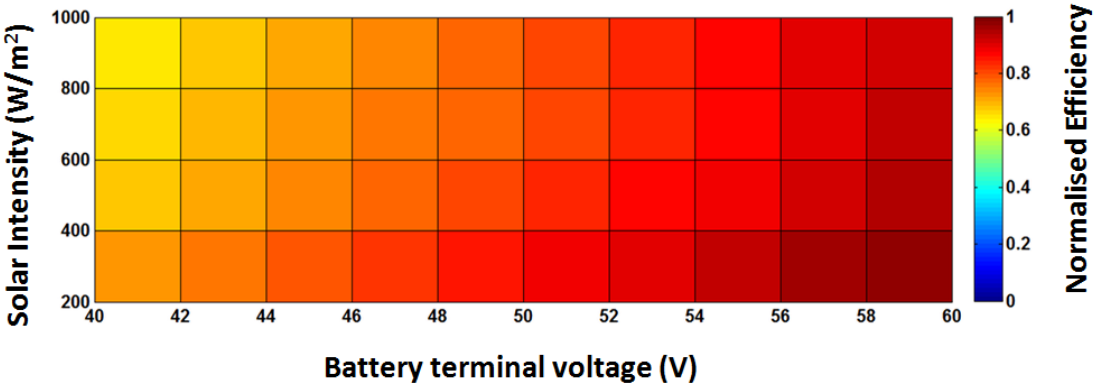

Figure 17 Efficiency map associated with direct connection of 10X13 panel configuration to battery terminals

For the 13X10 configuration, the maximum power point is always at or above the highest possible battery voltage (in this example 60V).

To determine the optimal point of operation, the controller operates along the lines of the following routine:

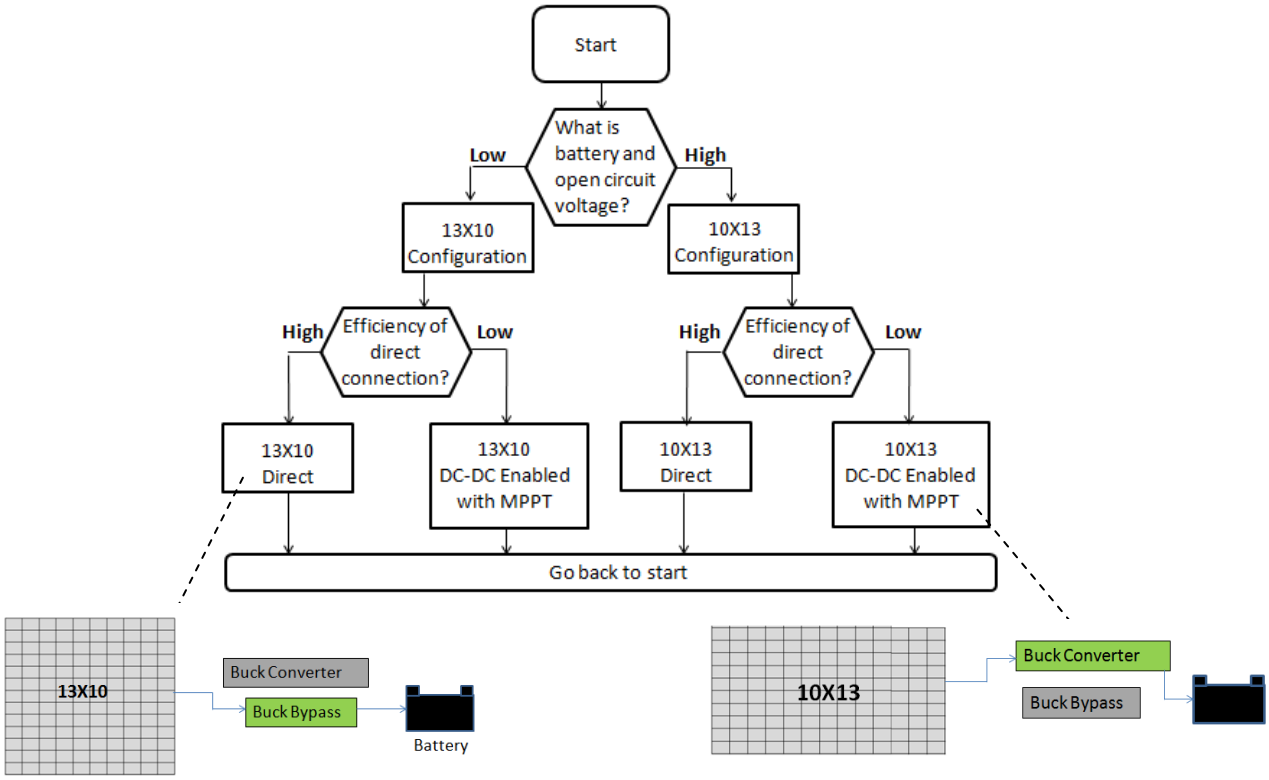

Figure 18 Routine associated with control of reconfigurable PV array and power electronics

The controller begins by examining the battery voltage to find the horizontal location on Figures 15 and 16. To determine solar insolation levels, the open circuit voltage is monitored and the known relationship between W/m^2 and V_{oc} (Figure 19) is utilised:

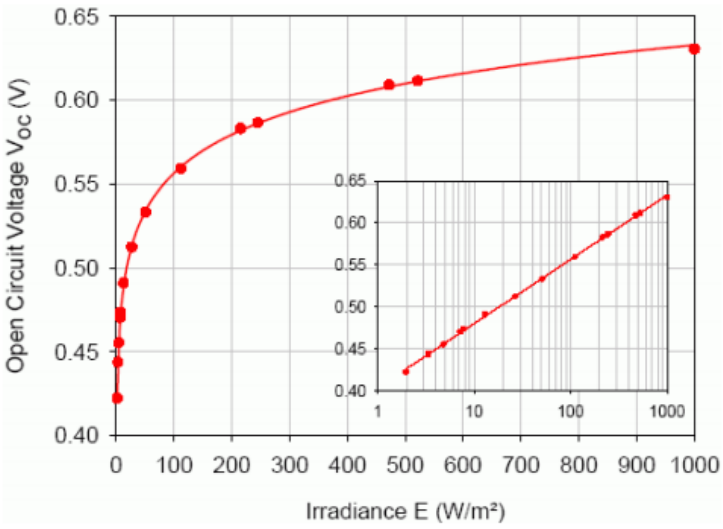

Figure 19 Relationship between open circuit voltage and Irradiance of solar cell

Using the knowledge of insolation and battery voltage, along with efficiency data of the DC-DC converter, the control routine depicted in Figure 18 selects the panel configuration and connection scheme according to the following operational map:

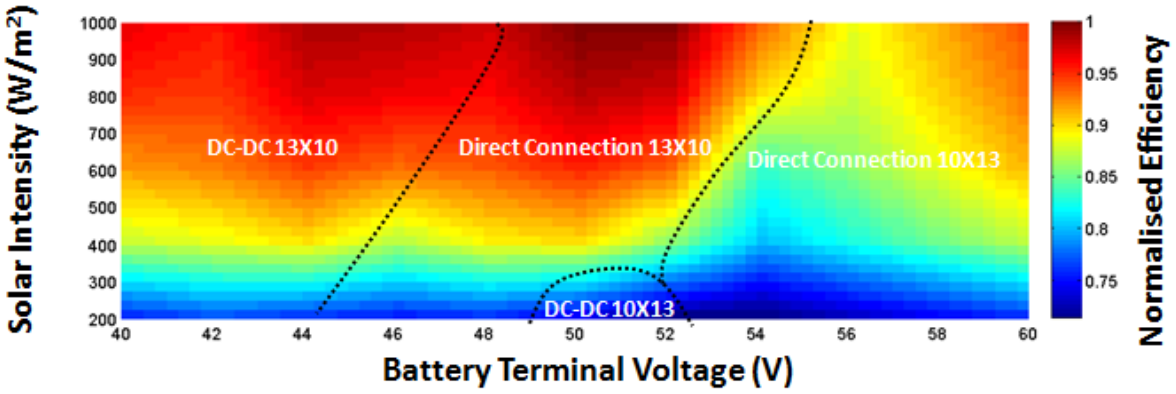

Figure 20 Operational and performance map of PV scheme from simulation data annotated to show configuration associated with maximum efficiency

Figure 20 shows each system configuration across a range of battery voltages and levels of solar irradiation. The dashed lines mark out the regions where each circuit and panel configuration is most efficient. Over a significant part of the operating map, direct connection proves most efficient, where the DC-DC converter is used, efficiency is higher due to the lower disparity between MPP voltage and battery terminal voltage.

1.6 Conclusions

There are two primary benefits associated with this scheme:

1. Improved efficiency where direct connection is possible

As can be seen in Figure 20, the most efficient modes of operation are associated with direct connection of the PV where the penalty associated with the DC-DC converter is outweighed by the advantage derived from maximum power point tracking.

2. Improved efficiency of DC-DC converter resulting from optimal PV configuration

Figure 4 shows the relationship between duty cycle and efficiency for a DC-DC converter. The duty cycle relates to the difference between input and output voltage according to Equation 1. The DC-DC converter is more efficient where the input and output voltages approach one another. By changing PV configuration, the voltage associated with maximum power transfer on the PV side can be brought closer to the battery terminal voltage therefore improving DC-DC converter efficiency.

The improvement in efficiency of the scheme above compared with the traditional scheme shown in Figure 3 can be as high as 5% depending on the battery terminal voltage and level of solar insolation.

1.7 Answers to Shell Technical Award Questions

This section will directly answer the list of questions posed by Shell®:

1. **How did you come up with the idea for the innovation (s)?**

The idea originated whilst looking at the large number of cells available on the market. It became evident that the panel area could be made up from many small cells so that the overall voltage current curve could be tuned to best match the battery terminal voltage, the logical extension of this was to develop a system which dynamically changed the number of cells to best suit the battery as the terminal voltage changed.

2. **Does this innovation involve original technical solutions or new materials in any of the following?: drive train, chassis, instrumentation, signal processing, engine optimisation, vehicle path optimisation, etc, or other functions (steering, brakes, etc)?**

This innovation relates to the power take off system associated with the PV.

3. **Has this innovation already been applied in other fields? Please specify.**

To the best knowledge of the team, this scheme has not been explored anywhere else. There could be many applications where PV is used in conjunction with electrochemical energy storage for both mobile and stationary applications.

4. **Does this innovation have a significant impact on improving fuel economy? If so, can you prove it and quantify the economy?**

Depending on the size of the PV array relative to the driveline requirements, this scheme could have a significant impact on fuel economy. The overall improvement in conversion efficiency from the PV array is in the order of 5%. This is significant when considering the resources that go into making incremental improvements each year in solar cell performance.

5. **Do you think that this innovation can be scaled up to the industrial level? Why?**

Yes, for two reasons:

5.1 There is increasing interest in the application of ultra low energy vehicles for personal transport. Examples of this include a novel American vehicle, referred to as the 'ELF' which integrates a PV array into the shell to supplement the batteries [6]. As governments adopt wider policies to promote electric vehicles (such as road tax and congestion charge exemptions in the UK), photovoltaic power take-off schemes which maximise the output of the PV array will become attractive.

5.2 Throughout the world there is increasing attention towards standalone DC-micro-grids. Such systems may be serviced by a variety of renewable inputs with electrochemical energy storage to provide balance between supply and demand. As the state of charge of the system changes, battery terminal voltage varies in response. This scheme would be as relevant in maximising power take off in these applications.

6. **How did you manage your project from the initial idea through to completion?**

On having the idea, the team analysed typical photovoltaic performance curves under different levels of sunlight against the variation in battery voltage possible within the team's electric vehicle. Additional data was found regarding the performance of DC-DC power electronics which improves as the ratio between input and output voltage drops. After analysing the concept, it was decided to proceed to the design stage. Two members of the team dedicated evenings and weekends to: specifying the system architecture, drawing up circuit diagrams, specifying and selecting components and building prototype circuitry.

7. **Did you work with any outside partners in developing your innovation? Who? Why?**

We have been sponsored in this effort by Future Electronics™ who donated the solar cells to us. We found there cells to be of the highest efficiency out of all the commercially available modules advertised.

8. **Do you have any other information that you would like to make known to the innovation judges?**

At this stage we have no further information to present, although we would welcome further questions from any members of the judging panel to clarify any aspects of our design and its performance.

9. **Do you wish to keep certain aspects of your innovation confidential? If so, please specify.**

No, we are happy for this information to become publicly available.

2. Phase-Locking Active Clutch System

2.1 Introduction to Phase-Locking Control Scheme

This year's driveline makes use of a set of dog clutches which disengages the output gear from the wheel hub so that the vehicle is able to coast freely. The value of the so called "pulse and glide" driving style, which exploits the use of a freewheel and clutching mechanism has been demonstrated on hybrid vehicles [7]. It was found by the team's 2012 Shell Eco-Marathon entry that such a scheme can improve efficiency by as much as 26% compared with direct drive. This year, a MAXON™ coreless DC-propulsion motor is used. This has the advantage that no magnetic field rotates within the stator when it is de-energised, leading to reduced iron losses when freewheeling [8],[9]. However, de-clutching the driveline provides further energy savings by removing losses associated with the bearings and gear mesh. Figure 21 to 23 illustrates the arrangement developed for 2013:

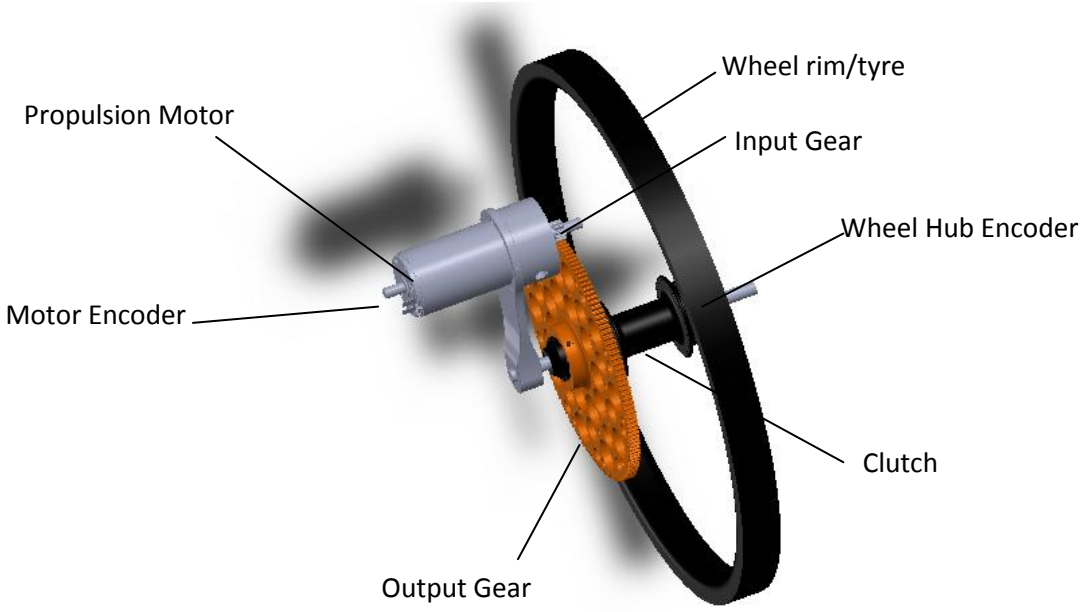

Figure 21 CAD model of vehicle drivetrain integrated on to rear wheel

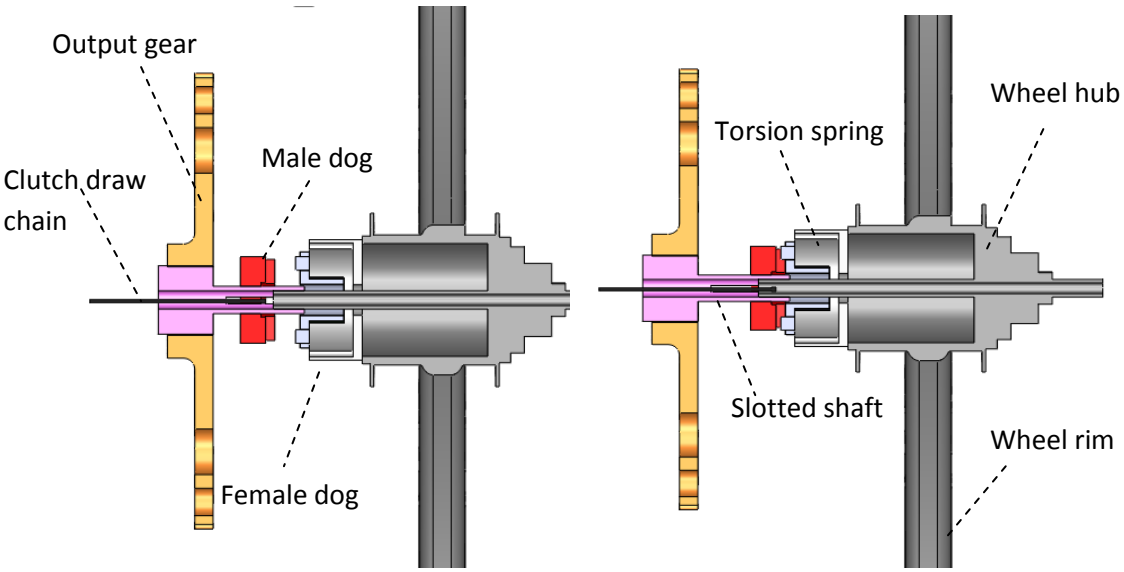

Figure 22 Exploded section view through 2013 driveline with clutch disengaged (left) and engaged (right)

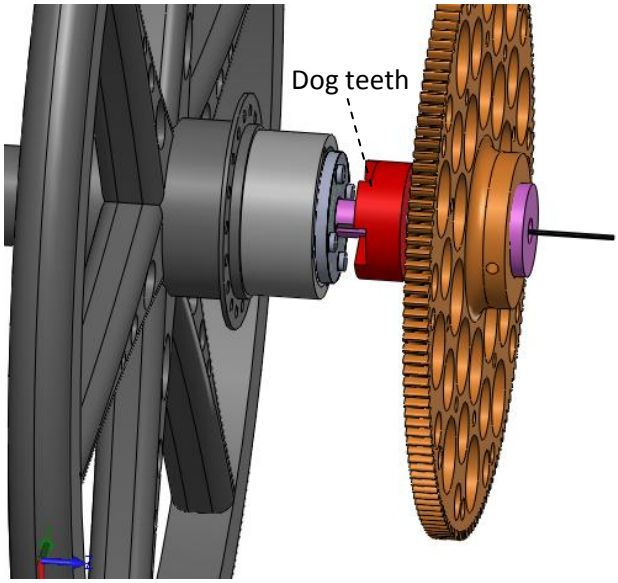

Figure 23 Exploded view showing dog clutches

The propulsion motor drives a spur gear stage. The output gear is connected to the wheel hub by a set of internal dog clutches. A motor encoder informs the controller of the speed and position of the output gear (via the gear ratio), and the wheel hub encoder monitors speed and position of the rear drive wheel.

Introducing a clutching mechanism brings in a number of technical issues which this scheme aims to address. The problems can be summarised as follows:

1. Where the engagement is manual, a mal-engagement (clutch engagement where there is a high relative speed between the motor and wheel), a large torque transient results leading to high stresses and risk of drive-line failure [10].
2. In order to reduce torque transients, some form of torsional flexibility is required, this leads to a mass penalty and also additional losses as hysteresis in the deforming materials (springs, rubber stops etc) results.
3. If an actuator is used along with a control routine to automate the engagement/disengagement process, a trade-off between speed of engagement, backlash in clutches, torque transient and actuator power consumption arises.

In this approach, positional feedback from the motor and wheel hub encoders, along with a phase locked loop control scheme, allows for the propulsion motor to target for the correct alignment at zero relative speed prior to engagement. As a result of this, an engagement is made without any torque transient, leading to the following benefits:

1. Reduced loading on driveline components
2. Removal of the requirement for torsional compliance leading to a stiffer drive-train and lower losses
3. Faster engagement as tooth alignment occurs alongside speed synchronisation of dog hubs
4. Actuator power requirements are reduced and the requirement for springs to decouple the actuator from the engagement mechanism during mal-engagements is no longer required.

2.2 System Diagram

The idea is illustrated by the system diagram shown in Figure 24. An encoder reference on the male and female dog clutches provides indication of speed and position. A control algorithm processes a throttle signal. If the throttle is in a neutral position, the controller will automatically disengage the clutch to allow the vehicle to coast without the losses associated with back-driving the spur gears and propulsion motor. When a demand for acceleration is made, the control algorithm demands torque from the motor via its controller so that the male dog is accelerated to the same speed and position as the female dog. The encoder references provide angular and positional velocity from which error signals are interpreted by the control algorithm. Once the speed and position of the dog hubs are synchronised, the actuator is commanded to proceed with engagement.

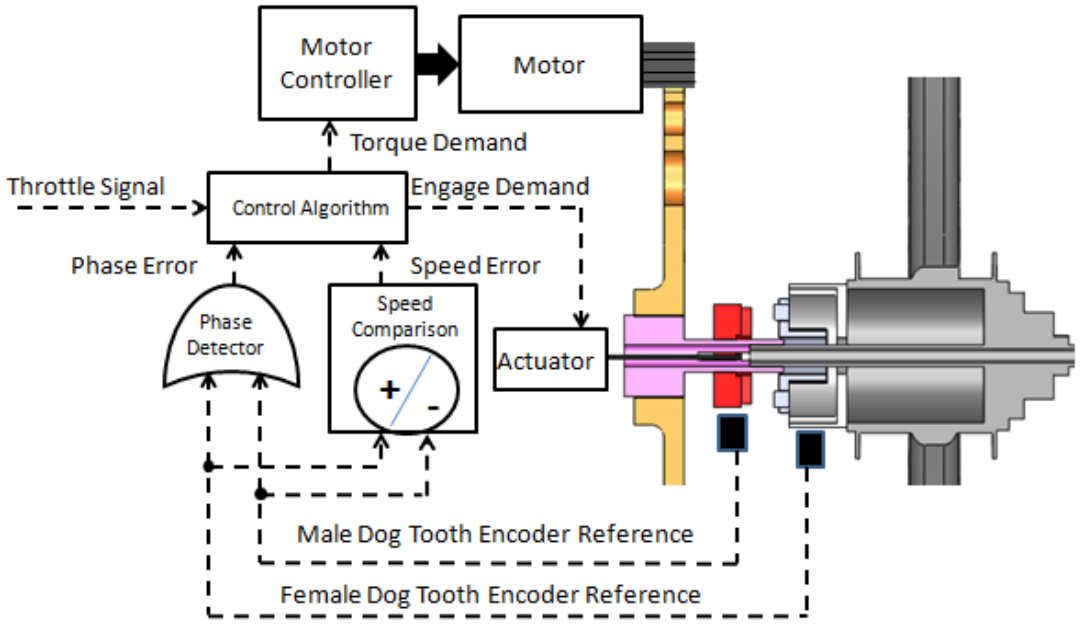

Figure 24 Phase locking active clutch system schematic

2.3 Simulation of Control Response

In order to understand the dynamics and control requirements of the scheme, a numerical simulation is presented in this section.

The control topology is similar to the architecture found in phase locked loops [11]. The dog tooth phase refers to the relative angular position of the male and female dog hubs. When the relative phase (or phase error) is zero, the dog teeth are aligned and can be engaged. Voltage controlled oscillators are used to synthesise the male and female dog tooth positions for the purposes of simulation in MATLAB Simulink®. The frequency associated with each oscillator is analogous to the rotational velocity of the respective dog hub. Key to the control scheme is the operation of the phase detector, this simulation uses an exclusive OR gate which merges the output gear and wheel hub encoder signals to produce a pulse whose width is proportional to the phase error between the teeth. This signal is filtered and amplified before going into the motor controller as a throttle demand (Figure 25). When the dogs are aligned, the output of the filtered exclusive OR gate signal

goes to zero. Other more elaborate phase detection schemes can achieve higher stability when the phase has been locked but with added complexity [12].

The following truth table provides the input output response for an exclusive OR gate whilst Figure 25 illustrates how the filtered response produces a phase error in proportion to the phase angle between two square waves.

Truth Table for an Exclusive OR Gate		
A (Male Hub Encoder Ref)	**B (Female Hub Encoder Ref)**	**Y (XOR Output)**
0	0	0
0	1	1
1	0	1
1	1	0

Table 1 Truth Table XOR gate

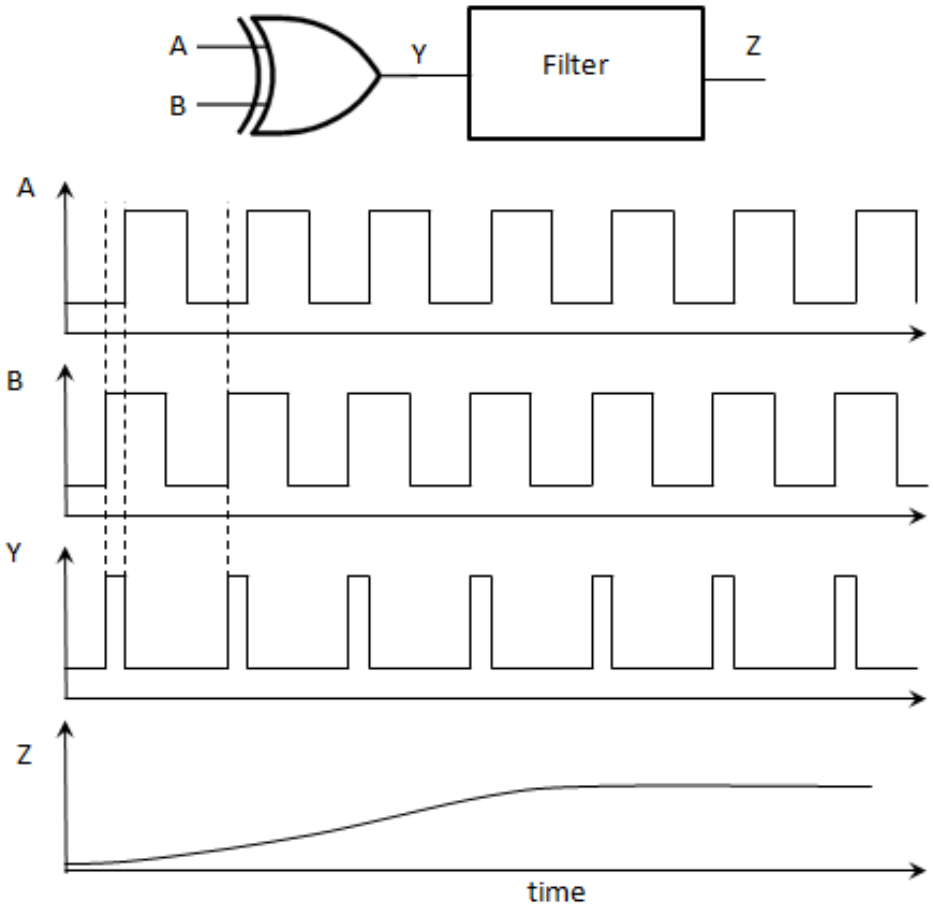

Figure 25 Illustration of use of XOR gate to detect phase between male and female dog hub references

Figure 26 provides the layout of the numerical simulation undertaken in Matlab Simulink® whilst Figure 27 provides the response of the system whilst the male dog is accelerated from rest to synchronise with the speed and phase of the female dog hub.

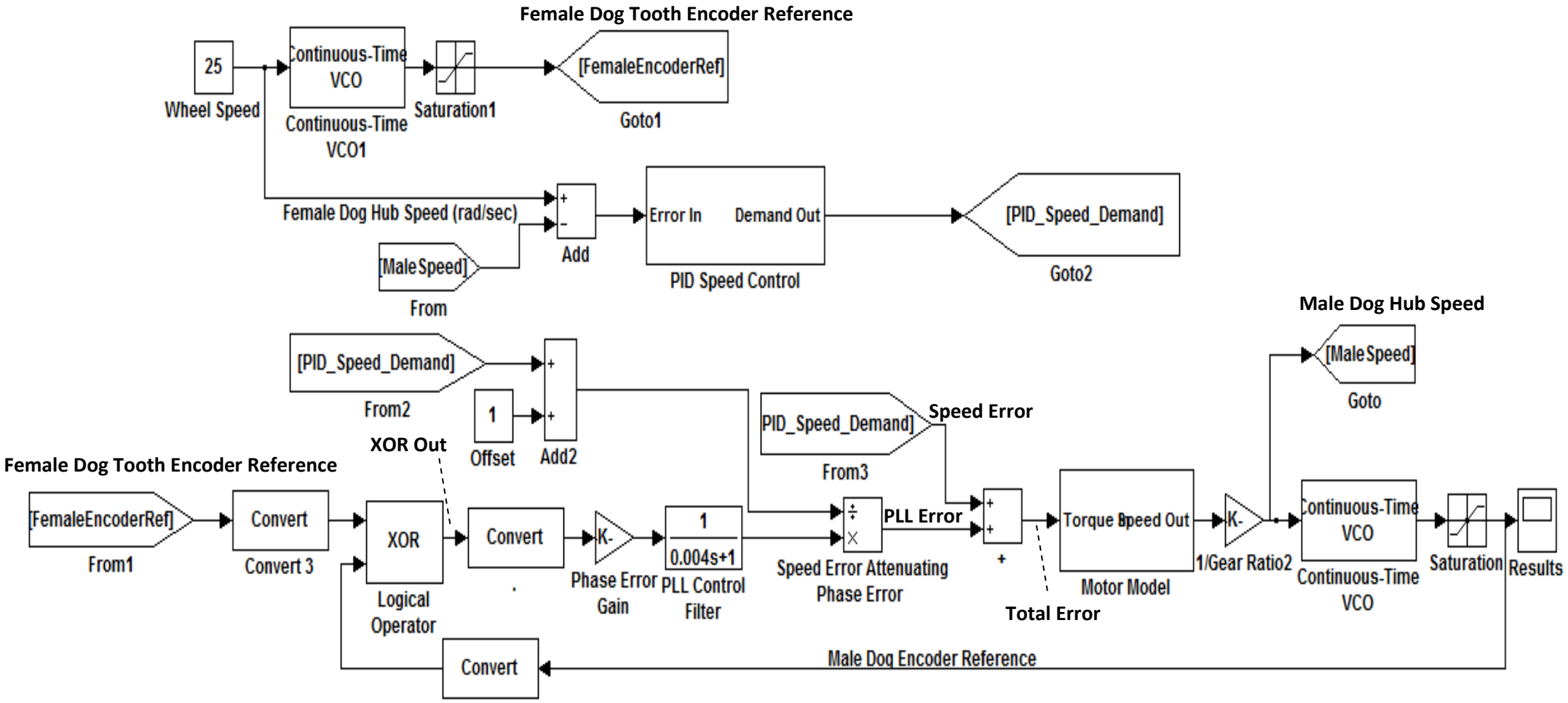

Figure 26 Matlab® simulation of phase locking active clutch system

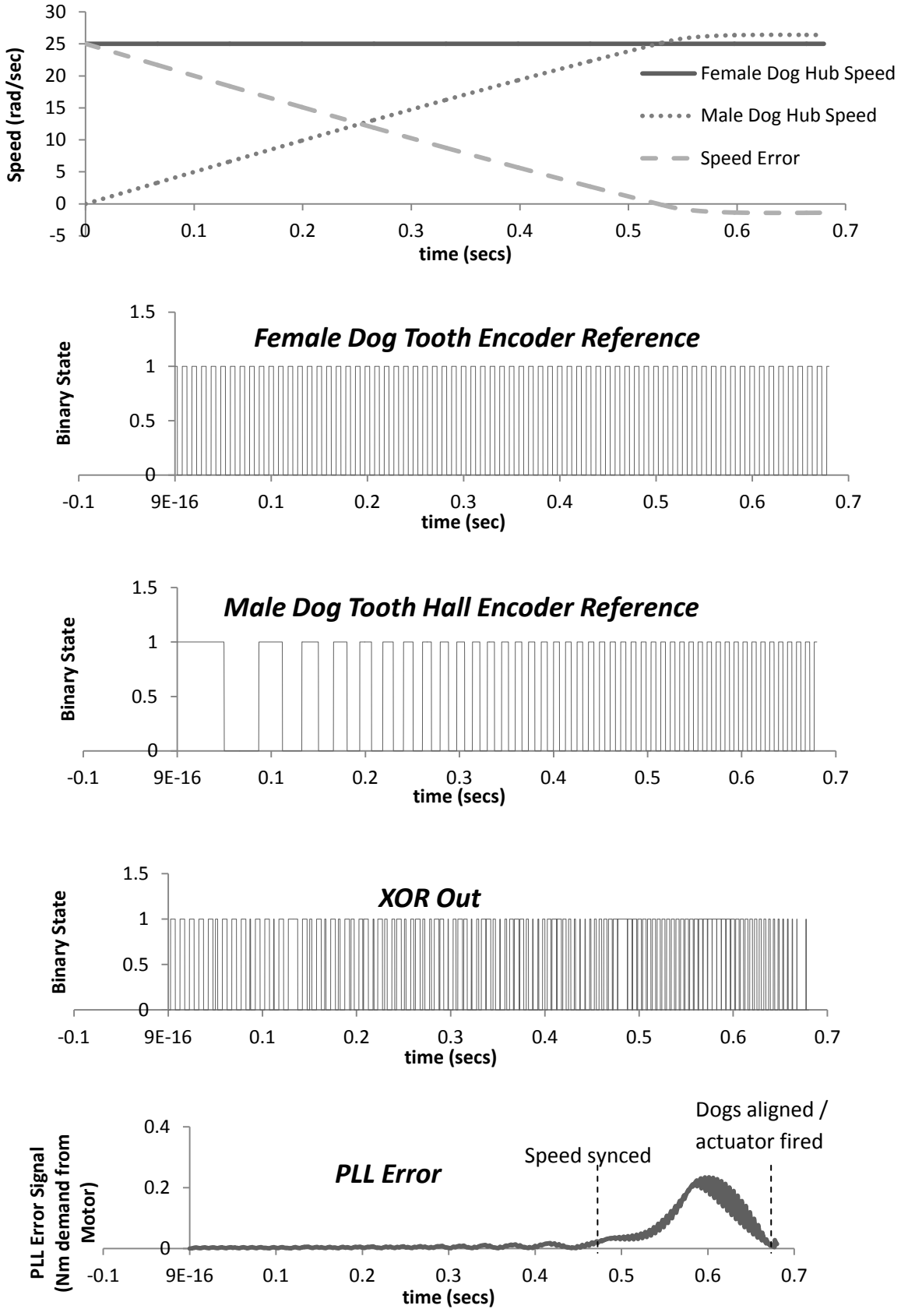

Figure 27 Dog Teeth Attaining Synchronism over time for a fixed wheel speed of 25 radians per second where motor starts from rest

The speed and phase errors are combined to form the Total Error which is fed into the motor controller. Initially the speed error is high, leading to a large demand from the motor controller. The speed error signal suppresses the phase error until speed synchronisation is achieved:

$$Total\ Error = Speed\ Error + \frac{Phase\ Error}{Speed\ Error + Offset}$$

Equation 4 Attenuation of speed phase error until speed has synchronised

Once speed synchronisation has been achieved, the Speed Error, is low and so consequently the Total Error becomes dominated by the phase error which drops off as the dog hubs align to the engagement position.

2.4 Quantifying Benefits of this Scheme

This section discusses the traditional dog-clutch control strategy along with the associated compromises and design challenges that arise. By quantifying these problems, a baseline is provided from which to assess the value of the proposed phase locking scheme.

The usual method of engaging dog clutches is simply to actuate the male hub against the female at some relative speed until they engage. A spring is usually required to decouple any axial bounce during mal-engagement.

1. Actuator requirements

Examination of the geometry of the dog teeth allows the actuator requirements for a given relative speed of engagement to be derived. Figure 28 shows the key geometric features that will be considered:

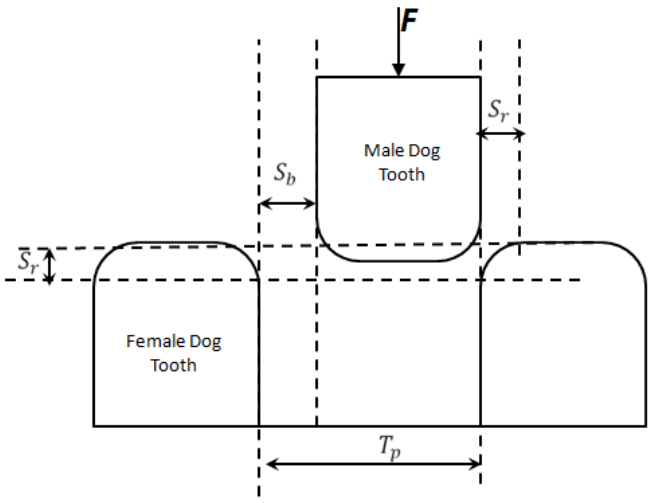

Figure 28 Dog tooth geometry which gives rise to actuator force requirements

For a given relative speed, Ω_{rel}, the dog teeth must engage within the window provided by the backlash S_b before the dog corner radius, S_r, is encountered. The corner radius is either machined into the teeth as a protection measure against high relative speed engagement events or to relieve contact stresses that arise. Square dogs will eventually develop rounded or worn corners depending on the amount of use and surface hardness. If the dog radii are encountered, the dog hub will likely

'bounce' backwards leading to a failed engagement and loading on any actuator protection springs. The threshold force, at which the corner radii can be cleared, has to be sufficient so that the following trajectory is followed by the dog hub.

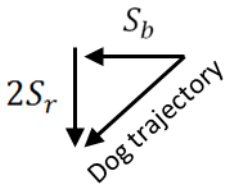

Figure 29 Vector diagram indicating dog travel required for successful engagement.

Typically, the dog will be driven by a pre-loaded spring, assuming zero friction and that the spring travel is small relative to its preload, we can derive the following force requirement:

$$F = \frac{4mS_r}{\left({}^{S_b}/_{\Omega_{rel}}\right)^2}$$

Equation 5 Force required to accelerate dog hub into engagement

Where F is the force acting on the male dog hub which has a mass of m. The geometry of the dog hubs within this year's driveline requires the following actuator force capability against tooth backlash and relative speed:

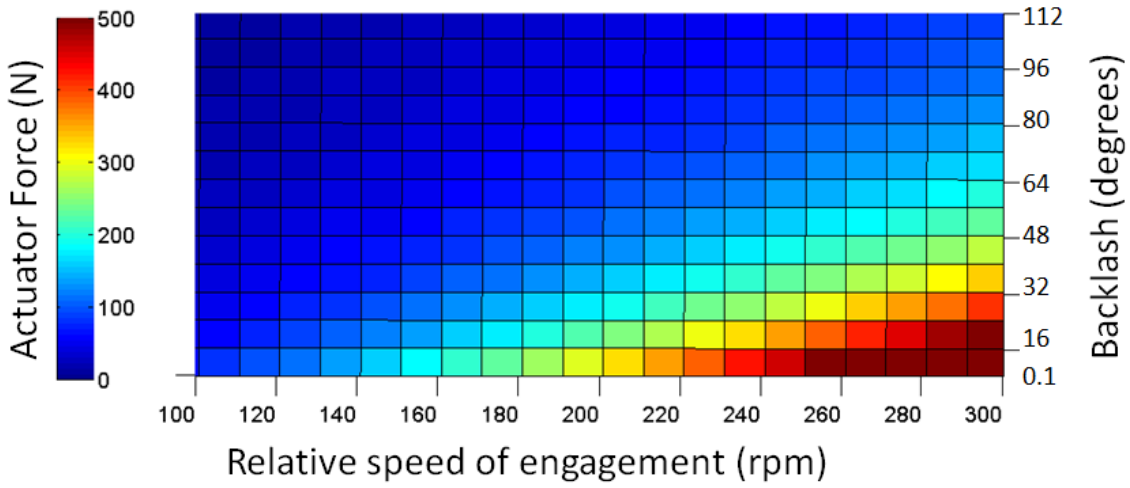

Figure 30 Relationship between relative speed, backlash and required actuator force

For fast engagement and a responsive driveline, high relative speed and low backlash is desired. However, as can be seen from Figure 30, the force requirements rise steeply as relative speed increases and backlash drops. An actuator meeting such requirements is heavy and consumes a significant amount of energy. The phase lock control strategy delivers the twin objectives of fast engagement and responsive driveline with minimal actuator requirements.

2. Torque transient and loading on driveline

Engaging at high relative speed leads to a large torque transient that can inflict damage on the driveline. If the loading is excessive, components have to be up-rated or torsional compliance needs to be added in response with a consequent increase in mass. This sub-section considers the likely loading on this vehicle and the consequences of adding torsional compliance.

We consider a step change in angular velocity applied to a single inertial lump which represents the combined inertia of the gear and referred motor inertia through a gear ratio N. We couple the inertial lump to a straight line lump representing the momentum of the vehicle giving the following coupled ODE (Equation 6 and Equation 7):

$$I_t \ddot{\emptyset}_1 + K_t(\emptyset_1 - \emptyset_2) = 0$$

Equation 6 ODE describing angular response of motor gear and torsional compliance within Peggie drivetrain during engagement event

Where I_t is the total inertia of the motor, input, output gears and male clutch assembly, $\emptyset_1$ is the angular position of the male dog with respect to a common reference shared by the female hub which rotates around $\emptyset_2$.

$$m\ddot{x} + \frac{K_t(\emptyset_2 - \emptyset_1)}{r} = 0$$

Equation 7 ODE describing straight-line response of vehicle during engagement event

Where:

$$I_t = I_{gear} + N^2 I_{motor}$$

Equation 8 Total inertia considered in analysis

Where N is the gear ratio and subscripts gear and motor refer to the respective inertias of the output gear and propulsion motor. The relation between the vehicle position x, wheel radius, r and angle $\emptyset_2$ is:

$$x = r\emptyset_2$$

Equation 9 Relationship between wheel angle and linear position of vehicle

The compliance of each component under consideration can be lumped as one spring with stiffness K_t operating according to Figure 31:

$$K_t = \left[\frac{1}{K_{gear}} + \frac{1}{K_{wheel}} + \frac{1}{K_{spring}}\right]^{-1}$$

Equation 10 Total compliance of Peggie driveline

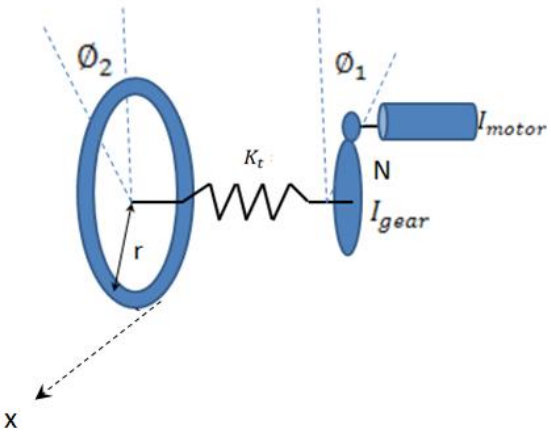

Figure 31 Illustration of Peggie driveline under analysis

To resolve individual component stiffness values, testing and finite element stress analysis was conducted. Figure 32 shows analysis conducted on the output gear to determine its stiffness.

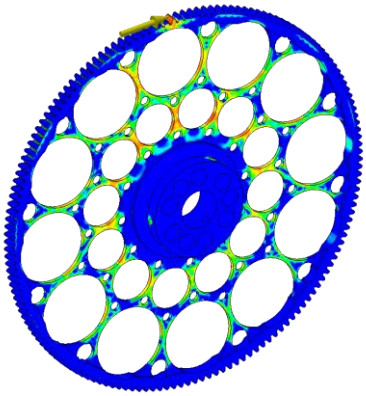

Figure 32 Normalised stress contours on gear under finite element analysis

Once an estimate of the total driveline stiffness had been arrived at, equations 6 and 7 were solved numerically for a worst case engagement scenario in which the vehicle, travelling at 30kmh, experiences an engagement attempt where the motor is initially at rest.

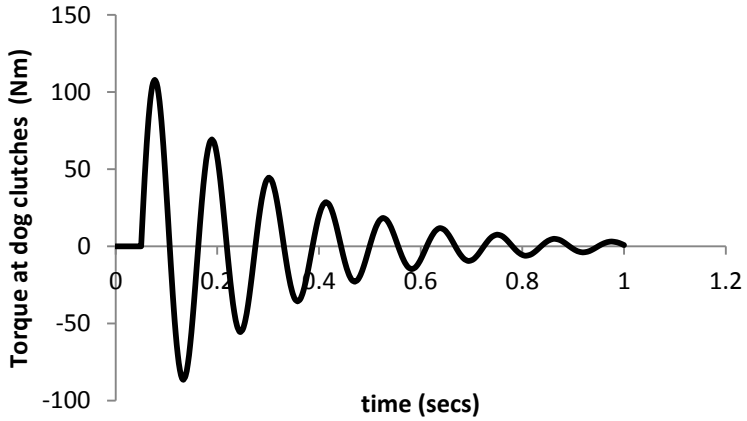

Figure 33Simulated driveline torque transient during worst case engagement

The resulting torque response, shown in Figure 33 indicates that additional compliance is required. As such, a torsion spring, with a stiffness of 60Nm/rad was designed providing the following estimated response which limited loading on the gears to acceptable levels:

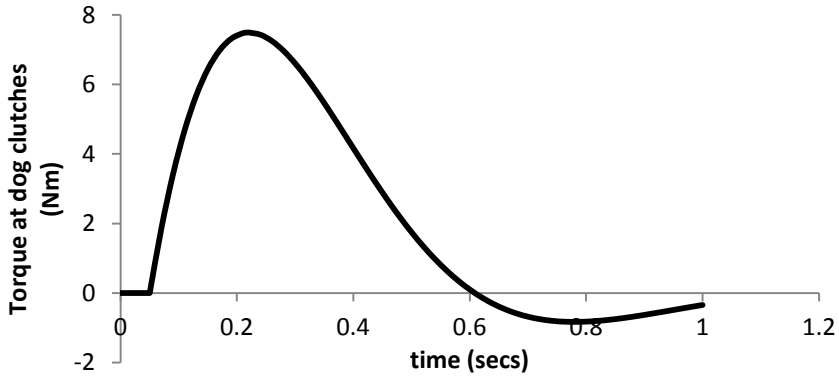

Figure 34 Torsional response of peggie driveline with a 60Nm/rad torsional spring

The hysteresis associated with the material used for the spring will consume energy. To assess the energy lost, we consider the following modifications which include the damping terms associated with the response in Figure 33:

$$I_t\ddot{\emptyset}_1 + C(\emptyset_1 \dot{-} \emptyset_2) + K_t(\emptyset_1 - \emptyset_2) = 0$$

Equation 11 Angular response including damping during an engagement event

$$m\ddot{x} + \frac{C(\emptyset_2 \dot{-} \emptyset_1)}{r} + \frac{K_t(\emptyset_2 - \emptyset_1)}{r} = 0$$

Equation 12 Straight line response of vehicle due to damping

The energy dissipated by the material can be estimated by:

$$E = \int_{t=0}^{\infty} C(\emptyset_1 \dot{-} \emptyset_2)^2 \, dt$$

Equation 13 Energy lost due to damping for a single engagement event

Figure 35 shows the resulting power and energy consumption associated with the spring:

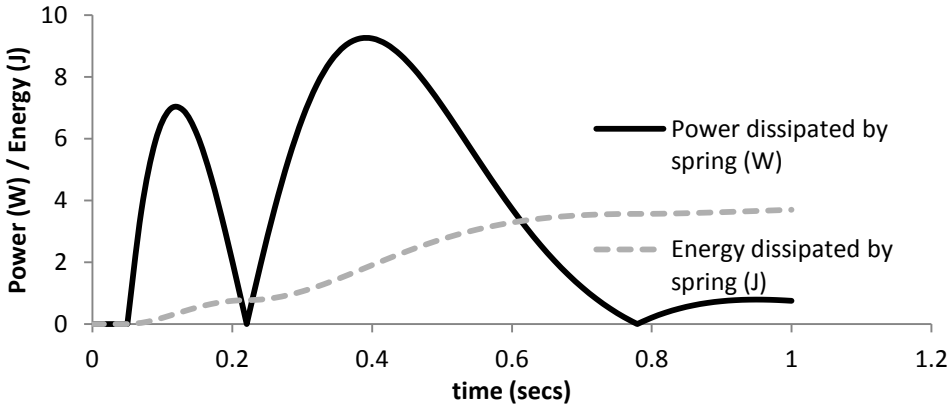

Figure 35 Power and energy dissipated inside spring as a result of hysteresis during an engagement

2.5 Conclusions

The analysis indicates that in order to achieve a quick engagement using dog hubs a significant amount of compliance has to be added to ensure that stresses do not exceed intolerable levels. Adding torsional compliance increases complexity, mass and overall losses due to the internal dissipation of energy within. Tight backlash, for a responsive driveline, requires high actuator force capability with consequent mass and energy consumption penalties. The phase lock gear control strategy enables engagement to occur at zero relative speed minimising the transient driveline torque, controlling to zero relative phase allows the backlash to be reduced leading to a responsive driveline with modest actuator requirements.

2.5 Answers to Shell Technical Award Questions

This section will directly answer the list of questions posed by Shell®:

1. **How did you come up with the idea for the innovation (s)?**

During testing, we found that the dogs struggled to engage without increasing the backlash. It then occurred to us that increasing backlash may permit very high speeds of engagement so we started trying to quantify the likely torsional response. We were frightened by the numbers so started work on a spring but then thought that a phase locking approach would be better.

2. **Does this innovation involve original technical solutions or new materials in any of the following?: drive train, chassis, instrumentation, signal processing, engine optimisation, vehicle path optimisation, etc, or other functions (steering, brakes, etc)?**

This innovation relates to the drivetrain.

3. **Has this innovation already been applied in other fields? Please specify.**

Phase locked loops are applied widely in electronics. The team is not aware of anyone who uses such a control strategy to facilitate clutch engagement.

4. **Does this innovation have a significant impact on improving fuel economy? If so, can you prove it and quantify the economy?**

Weight savings due to reduced actuator and compliance requirements are likely to save in the order of 1% total energy consumption, in addition, the reduced loss in any torsional damping may bring this figure up to 1.5% though this depends heavily on driving style.

5. **Do you think that this innovation can be scaled up to the industrial level? Why?**

Yes, for example the Volkswagon XL1 uses a clutch to enable freewheeling whilst the vehicle coasts and so would be a direct contender for this sort of scheme.

6. **How did you manage your project from the initial idea through to completion?**

Much of the project arose through chance, but once it was clear that aligning phase and relative speed prior to engagement was the goal, efforts were made to simulate the likely control response so that an algorithm could be developed for the hardware.

7. **Did you work with any outside partners in developing your innovation? Who? Why?**

No, we would have liked to have sought advice from companies like Ricardo, however time constraints prevented us from doing so.

8. **Do you have any other information that you would like to make known to the innovation judges?**

At this stage we have no further information to present, although we would welcome further questions from any members of the judging panel to clarify any aspects of our design and its performance.

9. **Do you wish to keep certain aspects of your innovation confidential? If so, please specify.**

No, we are happy for this information to become publicly available.

3. Real Time Feedback and Optimisation of Driving Strategy

3.1 Introduction to Scheme

Driving style is crucial to achieving low energy consumption. This section discusses an algorithm which develops an optimum driving strategy based on a dynamic straight line model of the vehicle, test data, and a map of the track. The algorithm has the objective of minimising energy consumption subject to the constraint that the vehicle maintains an average speed of 25kph and stays within safe cornering speeds. A free body diagram of the vehicle provides the threshold corner speed for a given turn radius. An analytical function is fitted to coast down data which can, in real time, be correlated with track position to account for variables such as prevailing head winds, track gradient, etc.

3.2 Algorithmic Procedure

The optimisation algorithm aims to provide an off-line solution by developing a predefined speed profile which minimises energy consumption subjected to a number of constraints including:

1. A minimum average speed of 25kph over the course of the race
2. Safe cornering speeds based on slip threshold for rear tyre
3. Motor speed and torque limits

The map of the race track is broken into a series of straights and corners, last year's example is provided by Figure 40 .

For each corner a speed constraint is computed. The coast profile of the vehicle is then fitted to the corner speed constraints as shown in **Error! Reference source not found.**.

We define the following three states of planar motion:

1. Acceleration:

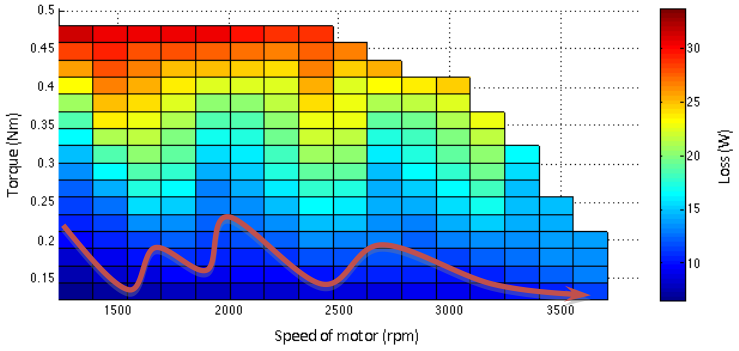

Figure 36 Illustration of trajectory sought by algorithm along torque, speed and loss map as vehicle accelerates

The algorithm searches for the path, which minimises the total energy loss, to reach the desired speed within a limited time.

Figure 36 illustrates the change in operating point for the propulsion motor as the vehicle accelerates from rest. During this period, torque is a variable that can be controlled whereas speed responds to torque according to the following relationship:

$$m_v\ddot{x} + \frac{1}{2}C_d\rho A\dot{x}^2 + \frac{C_\tau}{r_w}\dot{x} + m_v g\sin(\theta) + RRm_v g = \frac{\eta N\tau_m}{R_w} \rightarrow \dot{x}(t) \approx V_0 + \frac{\eta N\tau_m}{m_v R_w}t$$

Equation 14 Straight line vehicle response to applied motor torque and gear ratio

Where: m_v is vehicle mass, x is the linear path along which the vehicle travels, C_d is the aerodynamic drag coefficient, ρ is the density of air, A is the vehicle area, g is the acceleration due to gravity whilst θ is the gradient of the track, η is the driveline efficiency, N is the gear ratio, τ_m is the applied motor torque, RR is the tyre rolling resistance and R_w is the wheel radius. For high speed simulation, an approximation can be made from an initial speed V_0. The free body diagram used to derive the above relation is provided below:

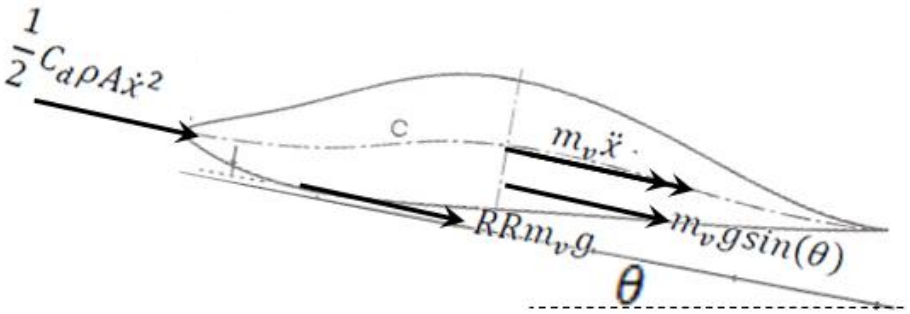

Figure 37 Free body diagram of vehicle used to derive straight line dynamics

2. Steady State

During steady state operation of the vehicle, the motor is operated along a low loss trajectory between two limits such that that the average speed of the vehicle is sufficient throughout the race. During steady state, the vehicle will reach a maximum speed before coasting (P_1). On reaching P_1, the clutch is disengaged allowing the vehicle to coast to a value (P_2), the vehicle then accelerates back to P_2. Whilst the vehicle is on the straight, it oscillates between P_1 and P_2.

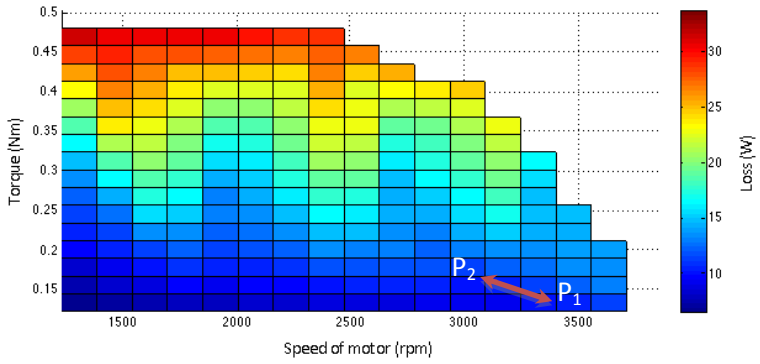

Figure 38 Illustration of trajectory sought by algorithm along torque, speed and loss map during steady state

3. Coast

As the vehicle approaches the corner, the vehicle will de-clutch the motor to allow freewheeling. In the first instance, the algorithm seeks to avoid braking, regenerative or otherwise unless the average speed requirement cannot be satisfied. Whilst coasting, the vehicle speed can be determined from:

$$m_v\ddot{x} + \frac{1}{2}C_d\rho A\dot{x}^2 + \frac{C_\tau}{r_w}\dot{x} + m_v g\sin(\theta) + RRm_v g = 0 \rightarrow \dot{x}(t) \approx V_0 e^{-\delta t}$$

Equation 15 Vehicle response during coasting with approximation

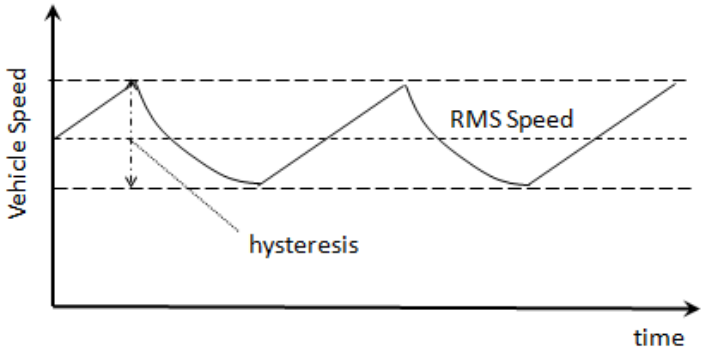

Figure 39 Illustration of straight line velocity profile between corners

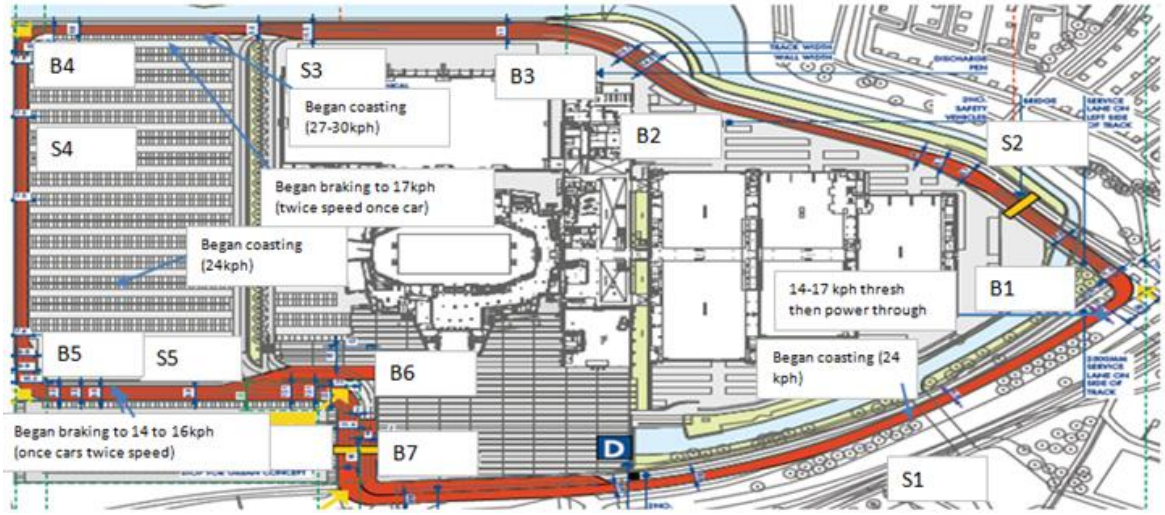

Figure 40 Identification of corners and straights for 2012 track

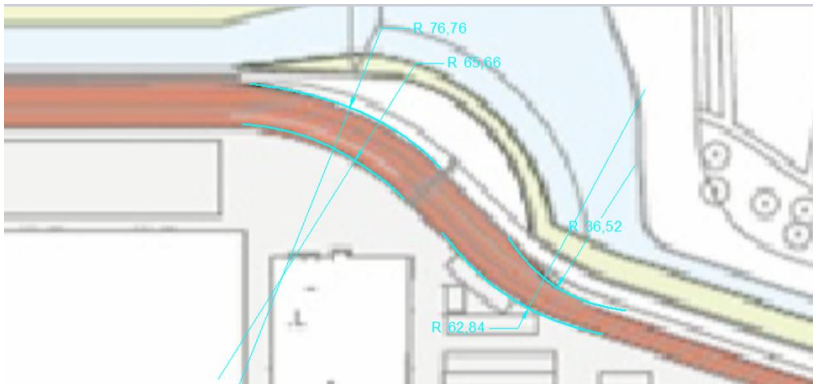

Figure 41 Example of corner identification and measurement

Figure 41 shows an example corner where the turn radii have been measured. The free body diagram shown in Figure 42 is used to define the maximum speed at which a corner can be negotiated. The speed is limited by the point at which the rear begins sliding due to the lateral force imposed by centripetal acceleration. The analysis considers the centre of the front axle as the fulcrum around which the vehicle pivots at maximum cornering speed. The friction coefficient associated with the rear tyre and road surface, along with the distribution of mass acting on the rear tyre influences the maximum cornering speed according to the following relation:

$$\frac{v_{thresh}^2}{r_t} x_m = \mu g C_r x_t$$

Equation 16 Equality at maximum cornering speed

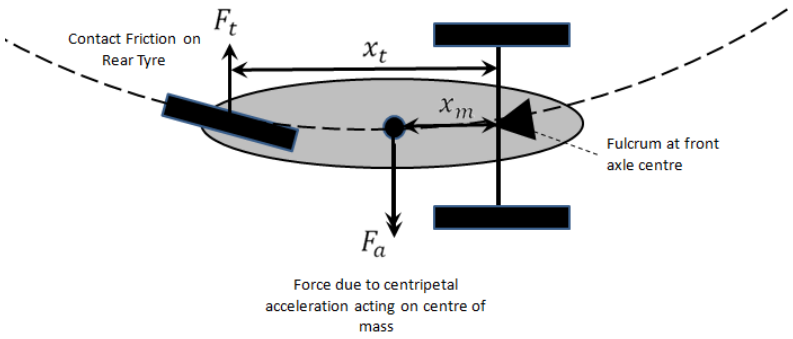

Figure 42 Free body diagram of vehicle undertaking a corner

Where V_{thresh} is the threshold velocity beyond which the vehicle will slide, r_t is the turn radius associated with the track, μ is the coefficient of friction between the rear tyre and road surface, g is the gravitational constant, C_r is the fraction of vehicle mass distributed over the rear tyre. x_m and x_t define the distance between the front axle centre and centre of mass and rear tyre contact point respectively. Equation 16 provides the following relationship between corner radius and maximum speed:

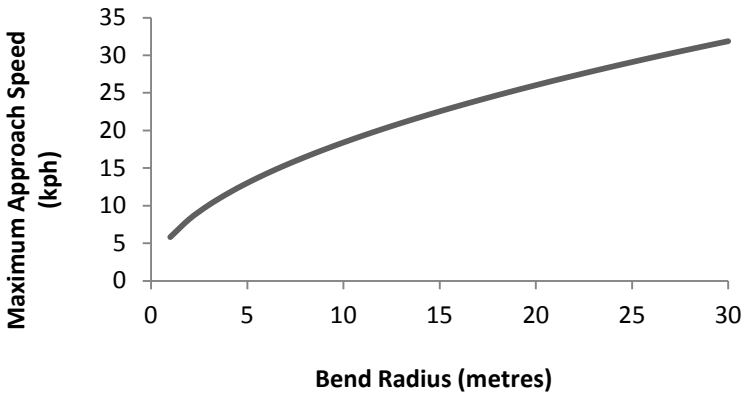

Figure 43 Relationship between bend radius and maximum cornering speed

Once the coast profiles have been fitted to the corner speed constraints, it defines the starting and finishing speed of the straight sections. The optimisation algorithm will then define the profile of the acceleration event and steady state (straight profile) such that minimum energy loss is attained.

The objective function during acceleration is to optimise the acceleration of the vehicle which minimise the energy loss (calculated from the integration of power w.r.t. time) as shown below:

$$\min_{a} \int P_{loss}\, dt$$

Equation 17 Objective relating to energy loss

Subject to:

i. Initial and final speeds of the straight profile. These are defined from the fitted coast profile.
ii. Fixed distance. The distance between the previous and the following coasting can be identified from the coast profile. That distance is the predefined variable for each straight profile.
iii. Maximum motor acceleration and speed. These are defined by the maximum rating of the motor and are physically constrained.
iv. Maximum time for each straight profile. This constraint is defined to ensure the capability of the vehicle to finish the race within the required time.

For a given straight profile, the optimisation algorithm splits the track into a series of time-distributed points. It starts with an initial set of vehicle acceleration events, a_1 to a_n, for each point. The speed of the vehicle at each operating point is calculated from the acceleration. The motor torque requirements are derived from the dynamic straight line model, detailed above. The motor torque and speed requirements are examined to ensure constraints are met. If constraints are breached, another set of vehicle acceleration events is generated. This process repeats to identify the feasibility of the result. Meanwhile, the power loss at each operating point is computed by mapping the torque and speed onto the loss map. The fitness value is then calculated based on the fitness function in equation 18. The optimisation algorithm stops when a set of vehicle acceleration, which is feasible (met the constraints) with minimum energy loss (gradient of fitness function at this point is approximately equal to zero), is found. The constrained nonlinear optimisation algorithm is based on the interior point algorithm.

$$\min_{a_1 \ldots a_n} \sum_{i=1}^{n} P_{loss} \Delta t$$

Equation 18 Fitness function

Where *n* = number of points in the straight profile

By taking a sufficiently large number of points, equation 18 will converge to equation 17.

From the set of vehicle acceleration events, speed and distance can be calculated through equation 19. The trapezoidal rule is used to perform the approximation for integration. Angular speed of the vehicle wheel ($\omega = {}^{v}/_{r_w}$).

$$v_{i+1} = v_i + \int_{t_i}^{t_{i+1}} a \, dt \approx v_i + \frac{a_{i+1} - a_i}{2\Delta t}$$

$$d_{i+1} = d_i + \int_{t_i}^{t_{i+1}} v \, dt \approx d_i + \frac{v_{i+1} - v_i}{2\Delta t}$$

Equation 19 Derivation of speed and distance from acceleration

The algorithm takes constraints in the form of equality to zero and less than zero, based on equation 19. The formulation of the optimisation problem with *n* time-distributed points is shown below. Since maximum time is implemented, the final condition can be achieved before full time range.

$$\min_{a_1 \ldots a_n} \sum_{i=1}^{n} P_{loss} \Delta t \text{ such that } \begin{cases} 0 \leq a \leq a_{max} \\ \begin{bmatrix} v - V_{max} \\ -v \\ D - d_n \end{bmatrix} \leq 0 \\ \begin{bmatrix} v_f - V_f \\ v_0 - V_0 \end{bmatrix} = 0 \; where \; d_f = D \end{cases}$$

Equation 20 Formulation of optimisation problem

Where: a_{max} and V_{max} are the maximum motor acceleration and speed constraint respectively, D is the distance to be travel within the straight profile, V_0 and V_f are the initial and final speed requirement respectively for the straight profile.

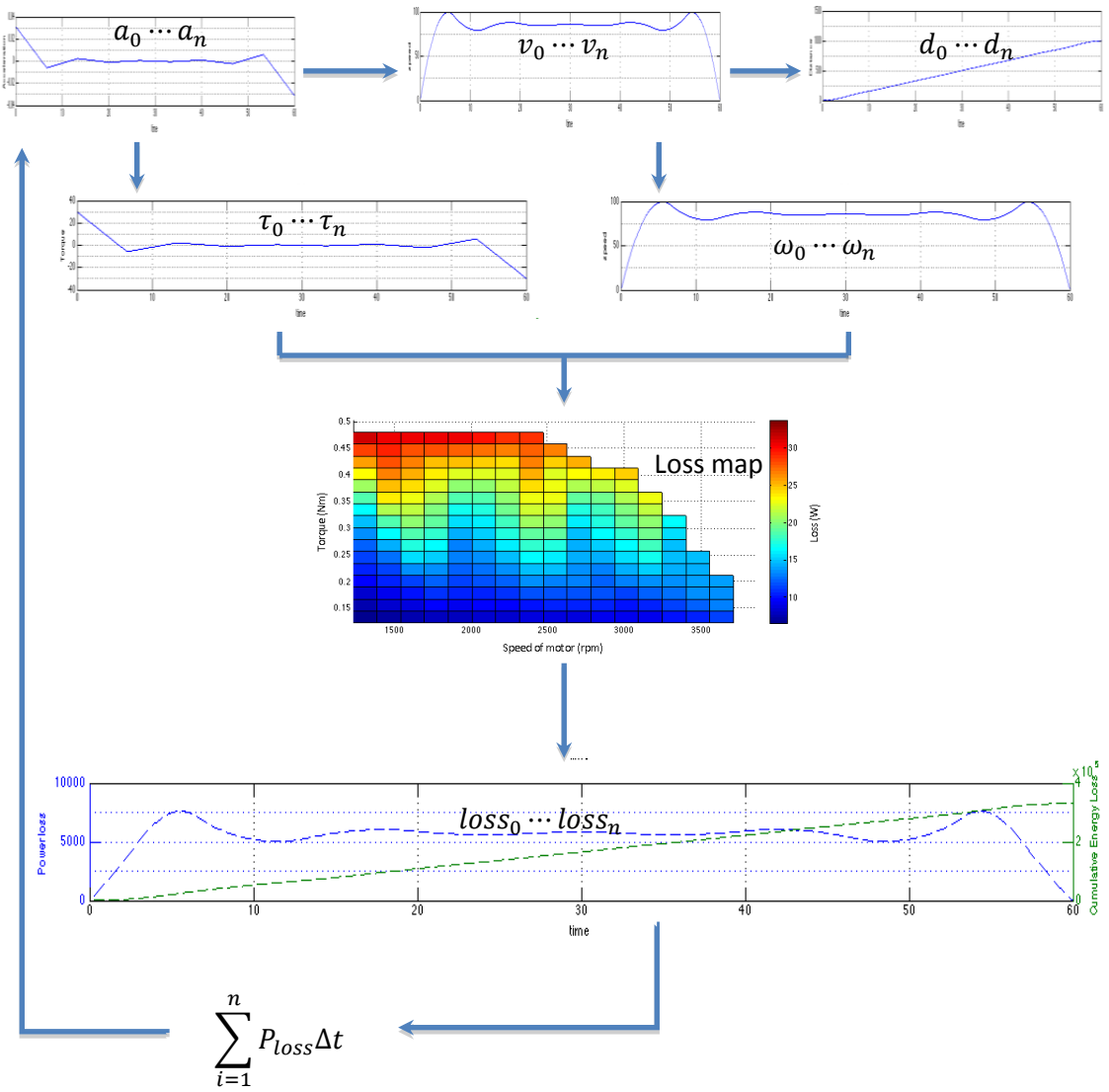

Figure 44 Illustration of operation of optimisation algorithm in Matlab

The acceleration to the straight line rms speed is determined by the optimal path through the torque speed efficiency map. Once corner speed constraints, rms speed and acceleration rates have been decided upon, the algorithm simulates the vehicle and checks whether all the constraints can be met without braking. If braking is required on any particular corner, the rms speed for that straight is reduced and automatically increased by a compensatory amount across the remaining straights. If the vehicle fails to attain the required average speed, a new global rms speed value is selected until all constraints are satisfied. Multiple rms speeds are simulated across the vehicle envelope. Once the vehicle envelope has been fully explored, the strategy associated with minimal energy consumption is selected.

Energy measurement data from the vehicle bus is fed back into the algorithm to compensate for changes in vehicle response that arise from head winds, slopes etc.

During the race, data acquisition system on the vehicle will provide information to improve the modelling of the track, vehicle response and driver response. This information is used to improve the constraint to fit the real world situation. Energy measurement data along the race is fed into the loss map to improve the modelling of the motor loss. The vehicle model is modified using the GPS data and the instantaneous motor torque and speed to fit the vehicle model to the situation at that particular day, i.e. to account for the head wind, slopes etc. in the model.

3.3 Driver Feedback

Whilst an offline approach is described to provide the driver with a pre-prepared strategy, during the race, the following map is provided on a mobile handset attached to the handle bars, providing feedback on efficiency, average time etc:

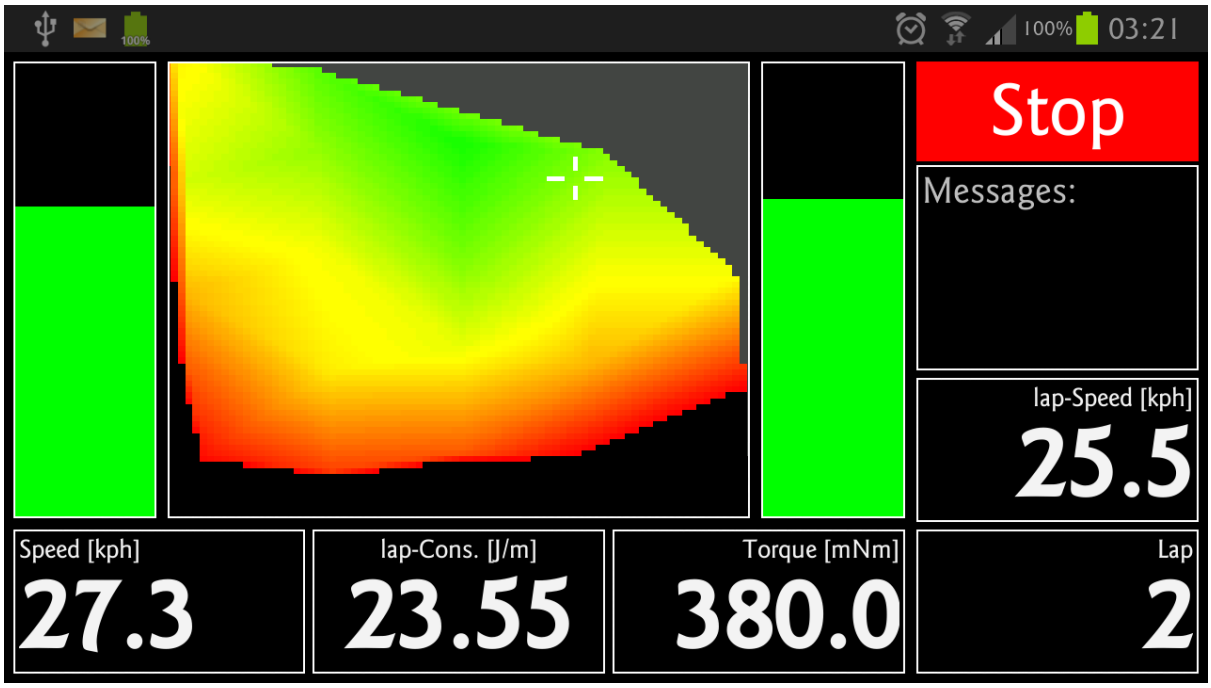

Figure 45 Driver display

3.3 Anticipated Energy Savings

It is difficult to predict energy savings, however it has been found that driving style can determine energy consumption by as much as 20% during the race.

3.4 Answers to Shell Technical Award Questions

This section will directly detail the list of questions in set out in the description of the technical innovation award provided by Shell®:

10. **How did you come up with the idea for the innovation (s)?**

It became apparent during testing that driving style had a significant effect on energy consumption.

11. **Does this innovation involve original technical solutions or new materials in any of the following?: drive train, chassis, instrumentation, signal processing, engine optimisation, vehicle path optimisation, etc, or other functions (steering, brakes, etc)?**

This innovation relates to the optimisation.

12. **Has this innovation already been applied in other fields? Please specify.**

Optimisation is used widely in many areas.

13. **Does this innovation have a significant impact on improving fuel economy? If so, can you prove it and quantify the economy?**

It is difficult to predict energy savings, however it has been found that driving style can determine energy consumption by as much as 20% during the race.

14. **Do you think that this innovation can be scaled up to the industrial level? Why?**

This would be easy to scale due to the availability of mobile handsets and vehicle data on modern CAN networks.

15. **How did you manage your project from the initial idea through to completion?**

A team member who is dealing with optimisation for their phd thesis worked on the project..

16. **Did you work with any outside partners in developing your innovation? Who? Why?**

No.

17. **Do you have any other information that you would like to make known to the innovation judges?**

At this stage we have no further information to present, although we would welcome further questions from any members of the judging panel to clarify any aspects of our design and its performance.

18. **Do you wish to keep certain aspects of your innovation confidential? If so, please specify.**

No, we are happy for this information to become publicly available.

4. References

[1] L. Castaner and S. Silvestre, *Modelling Photovoltaic Systems Using PSpice*. Chichester: John Wiley & Sons, LTD, 2002, p. 46.

[2] A. P. K. Yadav, S. Thirumaliah, and G. Haritha, "Comparison of MPPT Algorithms for DC-DC Converters Based PV Systems," vol. 1, no. 1, pp. 18–23, 2012.

[3] R. Ramaprabha and L. Mathur, B, "A Compact Maximum Power Point Tracking DC-DC Converter for Solar Photovoltaic System," *International Journal of Advanced Engineering Technology*, vol. III, no. I, pp. 133–140, 2012.

[4] D. W. Hart, "DC-DC- Converters," in *Introduction to Power Electronics*, Prentice Hall International Editions, 1997, p. 214.

[5] F. Ansari, A. Afzal, S. Chatterji, A. Iqbal, N. K. Nautiyal, and P. Thakur, "PSpice Model for Optimization of battery Charging using Maximum power point Tracker," pp. 2875–2882.

[6] "Here comes the cleanest, most efficient vehicle on the planet.," 2013. .

[7] J. Lee, "PhD Thesis: Vehicle Inertia Impact on Fuel Consumption of Conventional and Hybrid Electric Vehicles Using Acceleration and Coast Driving Strategy Vehicle Inertia Impact on Fuel Consumption of Conventional and Hybrid Electric Vehicles Using Acceleration an," Virginia Polytechic, 2009.

[8] M. Helmut, D. Jurgen, K. Hermann, S. Helmut, and T. Siegfried, *Small Electric Motors*, 1st Editio. London: Redwood Books, 1987, p. 165.

[9] M. Maxon, "Presentation on Maxon Coreless DC Permanent Magnet Motors," 2010. [Online]. Available: http://www.electromate.com/ftp/public/Maxon DC Motor Sizing Made Easy Presentation English Version March 2010/2_DcBldcMotor.pdf. [Accessed: 21-Mar-2013].

[10] P. D. Thesis, "Shifting Optimization of Face Dog Clutches in Heavy Duty Automated Mechanical Transmissions Supervisor : János Márialigeti," 2011.

[11] Analog_Devices, "Fundamentals of Phase Locked Loops (PLLs), Tutorial MT -086."

[12] D. Banerjee, *PLL Performance, Simulation and Design*, 2nd ed. Dog Ear Publishing, 2001, pp. 1–185.